AD-A047 418 NAVAL RESEARCH LAB WASHINGTON D C F/G 13/5
A METALLURGICAL CHARACTERIZATION AND ASSESSMENT OF SMA, GMA, EB--ETC(U)
SEP 77 J STOOP, E A METZBOWER

UNCLASSIFIED NRL-8157 SBIE-AD-E000 042 NL

1 OF 1
AD
A047418

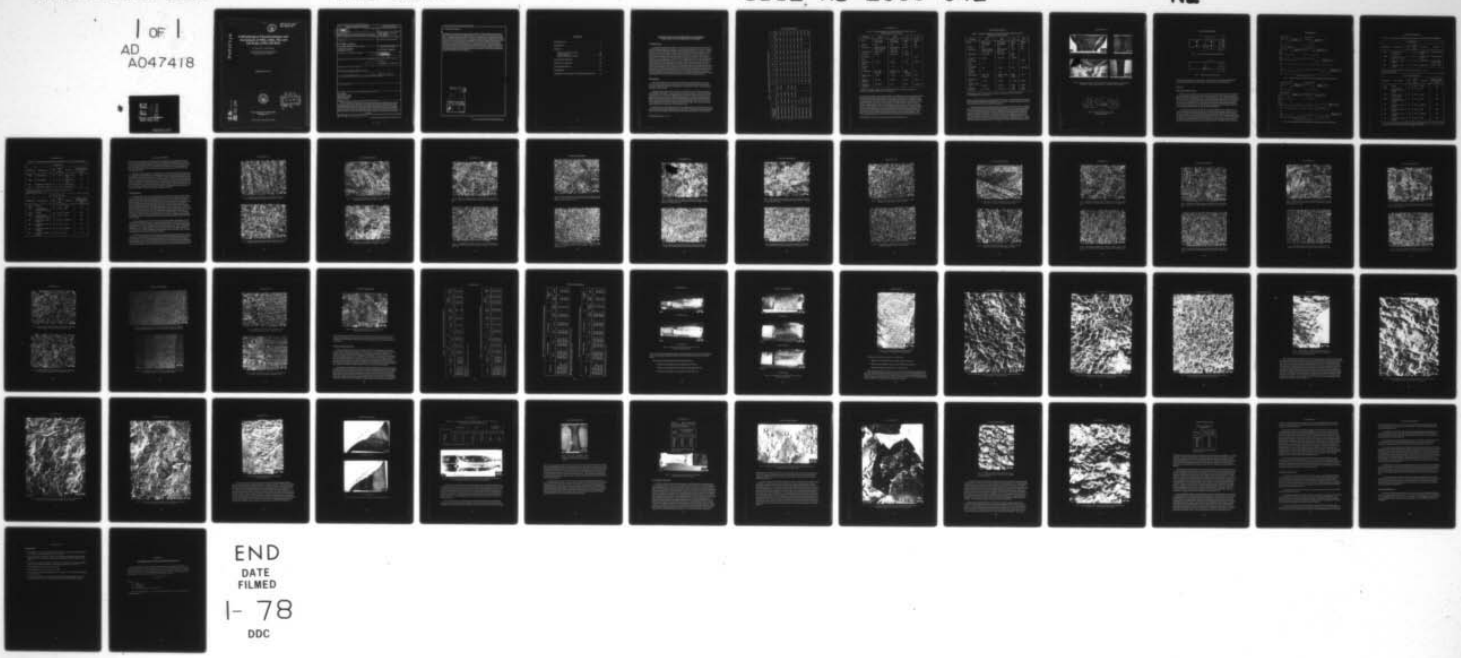

END
DATE
FILMED
1-78
DDC

NRL Report 8157

A Metallurgical Characterization and Assessment of SMA, GMA, EB, and LB Welds of HY-130 Steel

J. STOOP and E. A. METZBOWER

Advanced Materials Technology Branch
Engineering Materials Division

September 30, 1977

NAVAL RESEARCH LABORATORY
Washington, D.C.

SECURITY CLASSIFICATION OF THIS PAGE (When Data Entered)

REPORT DOCUMENTATION PAGE

READ INSTRUCTIONS BEFORE COMPLETING FORM

1. REPORT NUMBER: NRL [redacted]8157
2. GOVT ACCESSION NO.:
3. RECIPIENT'S CATALOG NUMBER:

4. TITLE (and Subtitle): A METALLURGICAL CHARACTERIZATION AND ASSESSMENT OF SMA, GMA, EB, AND LB WELDS OF HY-130 STEEL

5. TYPE OF REPORT & PERIOD COVERED: Interim report on a continuing NRL Problem

6. PERFORMING ORG. REPORT NUMBER:

7. AUTHOR(s): J. Stoop [redacted] E. A. Metzbower

8. CONTRACT OR GRANT NUMBER(s):

9. PERFORMING ORGANIZATION NAME AND ADDRESS: Naval Research Laboratory, Washington, D.C. 20375

10. PROGRAM ELEMENT, PROJECT, TASK AREA & WORK UNIT NUMBERS: NRL Problem No. 63M03-05

11. CONTROLLING OFFICE NAME AND ADDRESS:

12. REPORT DATE: Sep[redacted]77

13. NUMBER OF PAGES: 55

14. MONITORING AGENCY NAME & ADDRESS (if different from Controlling Office):

15. SECURITY CLASS. (of this report): Unclassified

15a. DECLASSIFICATION/DOWNGRADING SCHEDULE:

16. DISTRIBUTION STATEMENT (of this Report)

Approved for public release; distribution unlimited.

18 SBIE 19 AD-E[redacted]

17. DISTRIBUTION STATEMENT (of the abstract entered in Block 20, if different from Report)

18. SUPPLEMENTARY NOTES

19. KEY WORDS (Continue on reverse side if necessary and identify by block number)

Laser welding
Microstructure (metals)
Mechanical properties
Fracture toughness

20. ABSTRACT (Continue on reverse side if necessary and identify by block number)

HY-130 weldments of 6.35 and 12.7 mm thickness were fabricated by shielded metal arc (SMA), gas metal arc (GMA), electron beam (EB), and laser beam (LB) processes. Hardness explorations and metallographic examinations were made of the weld metal and heat-affected zone (HAZ) of the weldments. EB and LB weldments showed perceptibly higher weld metal hardnesses and steeper hardness gradients in the HAZ than corresponding SMA and GMA weldments. SMA and GMA welds consisted of a large percentage of acicular ferrite with smaller amounts of bainite and martensite; EB and LB welds

(Continue)

DD FORM 1 JAN 73 1473 EDITION OF 1 NOV 65 IS OBSOLETE
S/N 0102-014-6601

SECURITY CLASSIFICATION OF THIS PAGE (When Data Entered)

20. ABSTRACT (Continued)

comprised mostly martensite and a small percentage of bainite. Strain hardening exponent values for SMA, GMA, and LB welds were appreciably higher than the values obtained for EB welds and the base metal. As indicated by dynamic tear (DT) tests run at room temperature, the weld joint specimens exhibited mostly plane stress (slant) fracture. LB specimens disclosed a fracture toughness not only higher than that of the other weld joints but also comparable to the fracture toughness of the base metal. LB weld joint fracture energy values were found to be 94.5 to 97.7 percent of those of the base metal. Metallurgical conditions and variables that promote susceptibility to cold cracking were found to be more prevalent in SMA and GMA weldments than in EB and LB weldments. Inspection of the DT fractures disclosed a small to moderate amount of porosity in SMA and GMA weldments, the presence of cold shuts (incomplete fusion) in EB weldments, and some evidence on a minor scale of cold shuts and hydrogen embrittlement in the LB weldments.

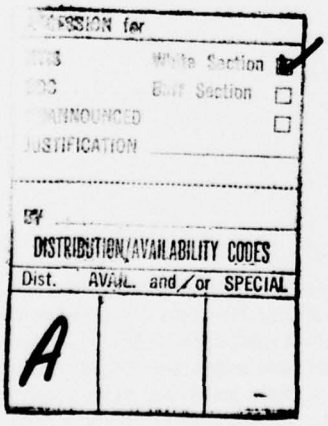

CONTENTS

A METALLURGICAL CHARACTERIZATION AND ASSESSMENT OF SMA, GMA, EB, AND LB WELDS OF HY-130 STEEL

INTRODUCTION

Quenched and tempered wrought HY-130 steel is a weldable high-strength material of exceptionally good resistance to fracture. In the welded condition, the steel can be made to equal or exceed the high yield strength and ultimate tensile strength it is capable of acquiring as a wrought or base metal. However, when welded by most fusion welding processes, the steel has a coarse, unworked, and partially refined structure, and therefore, may not achieve fracture resistance and ductility properties equivalent to those of the base metal. Moreover, in the welded state, the steel may be especially susceptible to cold cracking in the weld metal and heat affected zone (HAZ). Due to differences in basic welding techniques, variances in tensile properties, fracture resistance, and in hardness, as well as cold cracking susceptibility may result from different welding methods such as the shielded metal arc (SMA), the gas metal arc (GMA), the electron beam (EB), and the laser beam (LB) processes. A better understanding of the metallurgical factors influencing these parameters in HY-130 weldments may contribute significantly to achieving fracture-safe structures with optimum mechanical properties and low susceptibility to cold cracking. Essentially, the objective of this investigation was to explore and assess the mechanical properties and microstructural characteristics of HY-130 weldments fabricated by these fusion welding processes.

PROCEDURE

HY-130 weldments of 6.35- and 12.7-mm thicknesses were fabricated by the SMA, GMA, EB, and LB processes. The weldments were examined for defects by radiographic inspection. Base and weld metal compositions are presented in Table 1; welding details are given in Tables 2 and 3.

Transverse cross sections were cut from the weldments for microhardness testing and metallographic examination. Cross-sectional views of the weldments of 12.7-mm thickness are shown in Fig. 1. The weld configurations of the 6.35-mm weldments were found to be similar to those shown in Fig. 1. Hardness measurements were made in the mid-thickness region of the cross sections prepared for microexamination; a diamond pyramid indenter under a 300-gram load was used. The measurements were begun at the center of the weld and extended across the weld and HAZ into the unaffected base metal. The Vickers hardnesses obtained were converted to the Rockwell C scale.

Transverse weld tension specimens (Fig. 2) were machined from the weldments for testing at room temperature. Base metal specimens of the same configuration also were prepared so that a basis for comparison could be made with the weld joint specimens. The base metal

Manuscript submitted July 13, 1977.

Table 1 — Base and Weld Metal Compositions of HY-130 Steel (Wt %)

Sample Thickness (mm)	C	S	P	Mn	Ni	Cr	Mo	Si	V	Cu	Ti	Al
Base metal (6.35)	0.11	0.005	0.005	0.80	4.70	0.60	0.54	0.21	0.07	0.06	0.004	0.05
Base metal (12.7)	0.085	0.007	0.006	0.74	4.70	0.52	0.54	0.22	0.07	0.19	0.003	0.05
SMA weld (6.35)	0.073	0.006	—	1.02	4.30	0.62	0.66	0.27	0.03	0.04	0.02	0.02
SMA weld (12.7)	0.064	0.008	0.009	1.05	4.00	0.60	0.95	0.29	0.02	0.06	0.02	0.02
GMA weld (6.35)	0.11	0.006	0.007	1.30	3.60	0.72	0.84	0.33	0.03	0.06	0.01	0.02
GMA weld (12.7)	0.10	0.006	0.007	1.42	3.15	0.74	0.81	0.35	0.02	0.08	0.02	0.02
EB weld (6.35)	0.11	—	—	0.85	4.80	0.62	0.59	0.26	0.07	0.08	0.004	0.03
EB weld (12.7)	0.079	—	—	0.70	4.75	0.55	0.52	0.24	0.07	0.18	0.005	0.05
LB weld (6.35)	0.115	—	—	1.00	5.00	0.47	0.56	0.26	0.08	—	—	0.02
LB weld (12.7)	0.076	—	—	0.96	5.00	0.45	0.54	0.25	0.08	—	—	0.03

Table 2 — Welding Conditions for 6.35-mm-Thick SMA, GMA, EB, and LB Weldments of HY-130 Steel

Parameter	SMA	GMA	EB	LB
Joint	60°V groove 3.2-mm gap	60°V groove 3.2-mm gap	Square butt	Square butt
Position	Flat	Flat	Flat	Flat
Filler metal	E14018 4.0-mm-diam electrode	140 S 1.6-mm-diam wire	None	None
Amperage (A)	125, DCRP	300, DCRP	0.184	—
Voltage (V)	25-30	22.5-24.0	40,000	—
Power (kW)	—	—	—	8-12
Passes	3	3	1*	1
Travel speed mm/s	3.7-4.2	8.9-9.7	29.8	23-25
Wire feed mm/s	—	89	—	—
Environment	Gas + flux covering	Argon + 2%0_2 18.9 l/s	High Vacuum	He
Preheat temp (°C)	~ 120	~ 120	~ 120**	None
Interpass temp (°C)	95-150	95-150	None	None
Heat input (kJ/mm)	0.81-0.93	0.77	0.25	0.34-0.47

*Additional very light "cosmetic" passes were made for metal fill-in on surfaces of weldments.
**Two 6.35-mm-thick EB weldments were not preheated.

and weld joint specimens were machined with the longitudinal axes of the specimens aligned normal to the principal rolling direction of the plate. Strain gages were mounted on the specimens for obtaining yield strength, strain hardening exponent,* and modulus of elasticity measurements. On most occasions, a single strain gage was sufficient for each specimen and was mounted in the center of the specimen. In some instances it was necessary to mount two strain gages in series, one on each side of the specimen to cancel out bending stresses. Gages of either 3.17- or 6.35-mm gage length were bonded to the SMA and GMA weld joint specimens and the base metal specimens. Gages of 1.59-mm gage length were mounted only on the EB and LB weld joint specimens. Reference marks 50.8 mm apart were scribed on all specimens for subsequent measurement of percent elongation. The 50.8-mm gage length of each weld joint specimen spanned the weld extending from base

*See appendix for method used in determining strain hardening exponent values.

Table 3 — Welding Conditions for 12.7-mm-Thick SMA, GMA, EB, and LB Weldments of HY-130 Steel

Parameter	SMA	GMA	EB	LB
Joint	60°V groove 3.2-mm gap	60°V groove 3.2-mm gap	Square butt	Square butt
Position	Flat	Flat	Flat	Flat
Filler metal	E14018 4.0-mm-diam electrode	140 S 1.6-mm-diam wire	None	None
Amperage (A)	125, DCRP	300, DCRP	0.20-0.24	—
Voltage (V)	25-30	23.5-24.5	40,000	—
Power (kW)	—	—	—	10-11
Passes	7	5	1*	1
Travel speed (mm/s)	3.0	5.9-6.4	21.2	12.7-16.9
Wire feed (mm/s)	—	89	—	—
Environment	Gas + flux covering	Argon + 2%0_2 18.9 1/s	High vacuum	He, A
Preheat temp (°C)	~ 120	~ 120	~ 120**	None
Interpass temp (°C)	95-150	95-150	None	None
Heat input kJ/mm	1.10-1.18	1.14-1.18	0.38-0.51	0.65-0.79

*Additional very light "cosmetic" passes were made for metal fill-in on surfaces of weldments.
**One EB weldment was not preheated.

metal on one side of the weld to base metal on the other side. Load-elongation curves were obtained with the strain gages connected to an x-y recorder. The latter was used in conjunction with a load cell and a universal testing machine.

Dynamic tear (DT) base metal and weld joint specimens, both with the same configuration, were prepared for impact testing at room temperature in a double pendulum machine of 2712 N-m (2000 ft-lb) capacity. The DT weld joint specimens consisted of transverse cross sections from the different weldments, which were notched through the thickness along the centerline of the weld. To avoid the possibility of buckling, the specimens of 6.35-mm thickness were laminated for testing in the two-ply configuration (Fig. 3). The drawing of the full section DT specimen of 12.7-mm thickness is shown in Fig. 4. The DT weld joint and base metal specimens were machined with the notch aligned parallel (WR) to

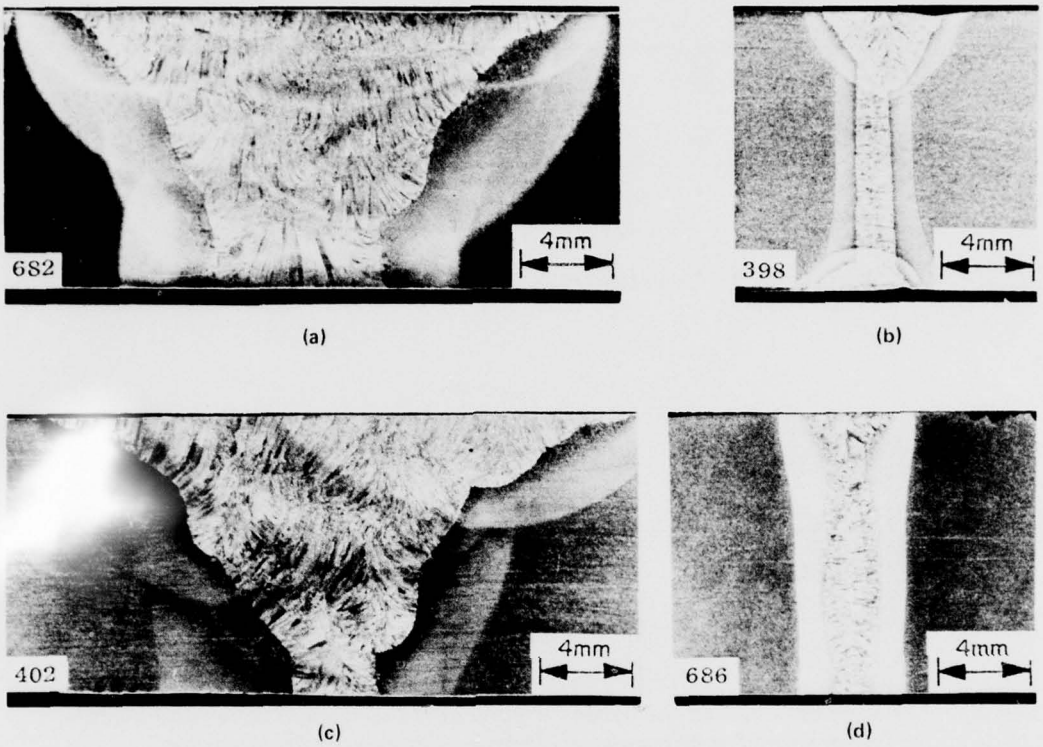

Fig. 1 — Cross-sectional views of 12.7-mm-thick HY-130 weldments etched in 10% ammonium persulphate: (A) SMA weld, (B) EB weld, (C) GMA weld, and (D) LB weld

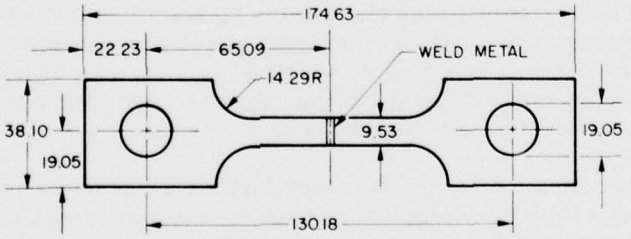

Fig. 2 — Transverse weld tension specimen (dimension in mm)

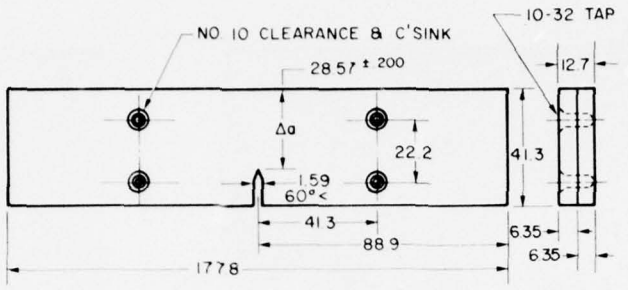

Fig. 3 — Laminated DT specimen (dimensions in mm)

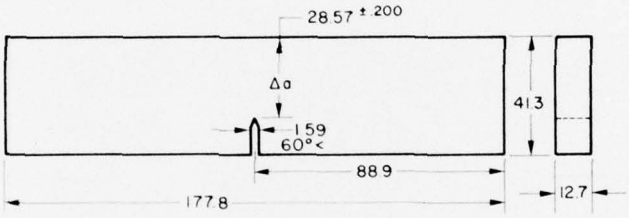

Fig. 4 — DT specimen (dimensions in mm)

the principal rolling direction of the plates. Fractured DT specimens were subsequently replicated for transmission for transmission electron microscope (TEM) studies.

RESULTS

Hardness and Microstructure

Hardness traverses which were made in the mid-thickness regions of the 6.35- and 12.7-mm-thick weldments are plotted in Figs. 5 and 6, respectively. The traverses demonstrate hardness variations and gradients in the weld and heat-affected zones. Weld metal hardnesses are shown to be at a perceptibly higher level for the EB and LB welds than for the SMA and GMA welds. The gradients in the HAZ of the SMA and GMA weld joints are moderately steep and in most instances show a gradual decline in hardness from high hardness levels. The EB and LB weldments of 6.35- and 12.7-mm thickness, however, revealed noticeably steeper hardness gradients than the SMA and GMA weldments.

In the HAZ of both the 6.35- and 12.7-mm thick weldments, two regions were considered of significance from the standpoint of microstructure, hardness, and grain size: (a) the structure adjacent to the fusion boundary; and (b) the fine-grain structure of highest hardness located most often beyond the midpoint of the HAZ. The microstructural data of the weld metal and the aforementioned regions of the HAZ in the 6.35- and 12.7-mm-thick weldments are compiled in Tables 4 and 5, respectively. Grain sizes in Tables 4 and 5 are expressed in relative terms such as fine, medium and coarse. Similarities in microstructure

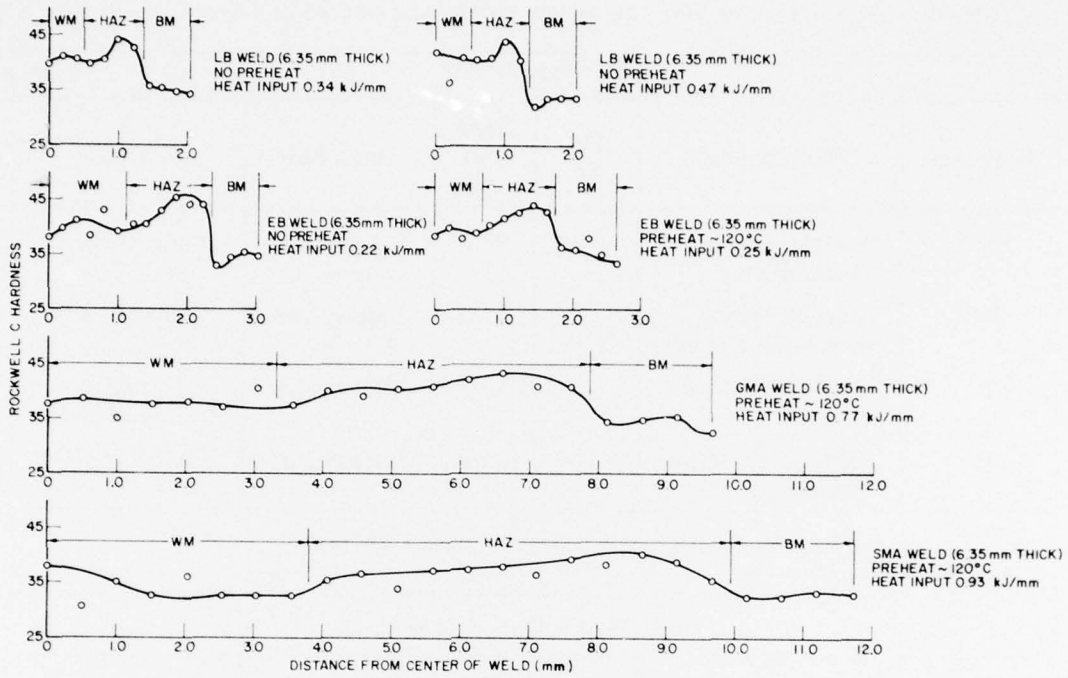

Fig. 5 — Hardness traverses of 6.35-mm-thick HY-130 SMA, GMA, EB, and LB weldments

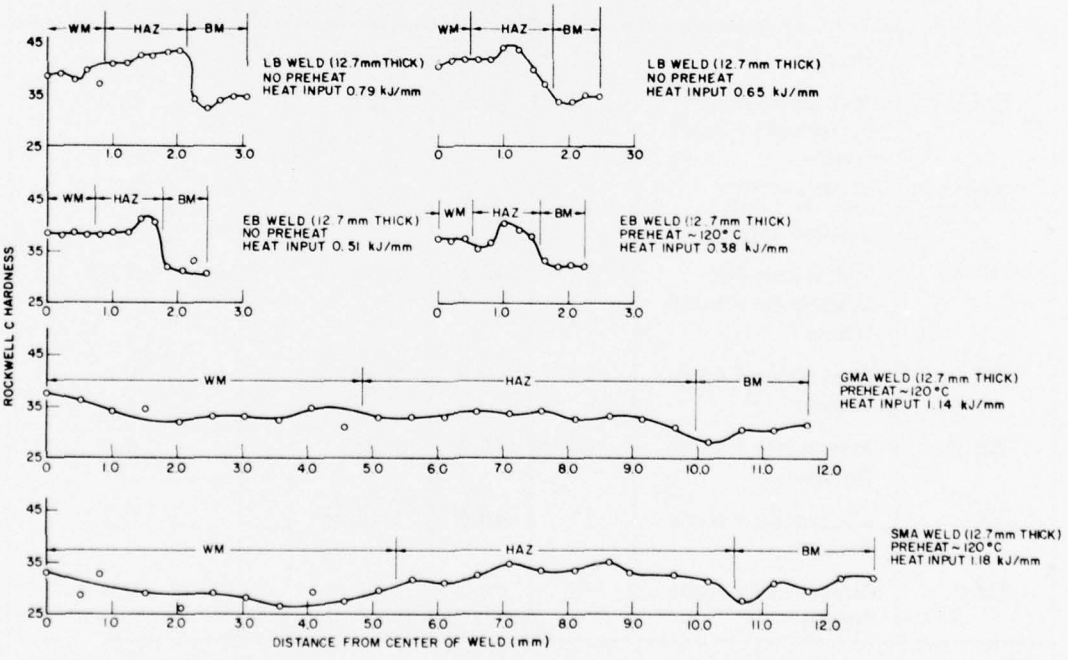

Fig. 6 — Hardness traverses of 12.7-mm-thick HY-130 SMA, GMA, EB, and LB weldments

Table 4 — Microstructures, Hardnesses, and Grain Sizes of 6.35-mm-Thick Weldments

A. Weld Metal*

Weldment	Microstructure	Fig. No.	Hardness (Rc)	Grain Size	Location
SMA	Acicular ferrite + martensite	7	38.0	Largely very coarse	Center of weld
GMA	Acicular ferrite, martensite + bainite	8	37.5	Largely very coarse	Center of weld
EB	Martensite + some bainite	9	43.0	Medium-fine	0.8 mm from center of weld
LB†	Martensite + some bainite	10	42.0	Largely fine	Center of weld

*EB and LB weldments not preheated. Other weldments preheated ~ 120°C.
†Heat input 0.47 kJ/mm

B. Heat Affected Zone†

Weldment	Microstructure	Fig. No.	Hardness (Rc)	Grain Size	Distance From Fusion Boundary (mm)
SMA	Bainite	11	36.5	Coarse	1.0
SMA	Autotempered martensite + some ferrite	12	40.5	Fine	5.1
GMA	Bainite + some acicular ferrite	13	37.5	Coarse	0.5
GMA	Autotempered martensite + some ferrite	14	43.5	Fine	3.5
EB	Martensite + some bainite	15	40.5	Medium	0.2
EB	Martensite + some ferrite	16	45.5	Fine	0.8
LB	Martensite + some bainite	17	40.5	Medium	0.2
LB	Martensite + some ferrite	18	44.0	Fine	0.6

†Two areas of each weldment were examined: (1) the coarse grain region adjacent to the fusion boundary and (2) the fine grain region showing the highest hardness of the HAZ.

Table 5 — Microstructures, Hardnesses, and Grain Sizes of 12.7-mm-Thick Weldments

A. Weld Metal*

Weldment	Microstructure	Fig. No.	Hardness (Rc)	Grain Size	Distance From Center of Weld (mm)
SMA	Acicular ferrite	19	26.0	Largely very coarse	2.0
GMA	Acicular ferrite	20	33.0	Largely very coarse	2.5
EB	Martensite + bainite	21	37.5	Medium-fine	0.4
LB†	Martensite + bainite	22	38.5	Medium-fine	0.0

*EB and LB weldments not preheated. Other weldments preheated ~ 120°C.
†Heat input 0.79 kJ/mm.

B. Heat Affected Zone

Weldment	Microstructure	Fig. No.	Hardness (Rc)	Grain Size	Distance From Fusion Boundary (mm)
SMA	Bainite	23	31.5	Coarse	0.5
SMA	Autotempered martensite + ferrite	24	35.0	Fine	3.5
GMA	Bainite	25	33.0	Coarse	0.5
GMA	Autotempered Martensite + ferrite	26	34.0	Fine	3.0
EB	Martensite + some bainite	27	38.0	Medium	0.2
EB	Martensite + some ferrite	28	41.0	Fine	0.8
LB	Martensite + some bainite	29	41.0	Medium	0.4
LB	Martensite + some ferrite	30	43.5	Fine	1.2

were found to exist between the SMA and GMA weldments of each thickness as well as between corresponding EB and LB weldments. Weld and HAZ microstructures representative of the 6.35-mm-thick weldments and those representative of the 12.7-mm-thick weldments are illustrated in Figs. 7 to 18 and 19 to 30, respectively. The microstructures in Figs. 31 and 32 are typical of the unaffected base metal structures of the 6.35- and 12.7-mm-thick weldments.

Although the SMA welds were comparable to the GMA welds, and the EB welds to the LB welds, some notable differences in microstructure were observed between similar welds. The EB welds of 6.35-mm thickness, for example, revealed a coarser solidification structure than the LB welds of the same thickness, as depicted in Figs. 33 and 34. No significant differences in solidification structure, however, were detected between the EB and LB welds of 12.7-mm thickness. The latter structures were comparable to the EB structures of the 6.35-mm-thick weldments. Note the relatively fine microstructures at the weld metal-HAZ interface of the EB and LB weld joints in Figs. 35 and 36 as compared with the coarse weld metal-HAZ interface structure for the SMA weldment in Fig. 37.

Tensile Properties

The tensile data of the base metal and transverse weld tension specimens of the 6.35- and 12.7-mm-thick weldments are presented in Tables 6 and 7. The SMA weld joint specimens were the only ones which fractured in the weld metal. This was due to the lower tensile strength of the SMA weld as compared with the tensile strength of the adjacent base metal. The specimens obtained from the 6.35-mm-thick weldments in most instances revealed strength levels substantially higher than those of the 12.7-mm-thick weldments. This was largely attributable to the higher hardenability of the 6.35-mm plates. The SMA and GMA welds showed the lowest and highest values of yield strength, respectively, in both the 6.35- and 12.7-mm thicknesses. The yield strength ranges for these thicknesses were 799.1 to 1017.0 MPa (115.9 to 147.5 ksi) and 811.5 to 916.3 MPa (117.7 to 132.9 ksi). Although the EB and LB welds of 6.35-mm thickness revealed comparable yield strengths, the EB welds of 12.7-mm thickness disclosed a yield strength appreciably higher than that of the LB welds.

The base metal plates of 6.35- and 12.7-mm thickness differed significantly in their elongation and reduction of area. The especially high reduction of area for the 12.7-mm thick plates showed that considerable necking had taken place. The correspondingly high elongation measured for the material was not uniform and evidently was to a large degree attributable to the marked necking. Weld defects, particularly those related to porosity, contributed to low values of elongation and reduction of area in the SMA welds. This was especially evident in the welds of 6.35-mm thickness.

The EB welds of both thicknesses disclosed strain hardening exponent values comparable to those of the base metal. On the other hand, the strain hardening exponent value for the GMA welds of 12.7-mm thickness and especially those of the SMA and LB welds of both thicknesses were substantially higher than the values obtained for the corresponding base metal thicknesses. However, it should be noted that since the GMA, EB, and LB weld joint specimens fractured in the base metal, frequently only limited or partial extension of

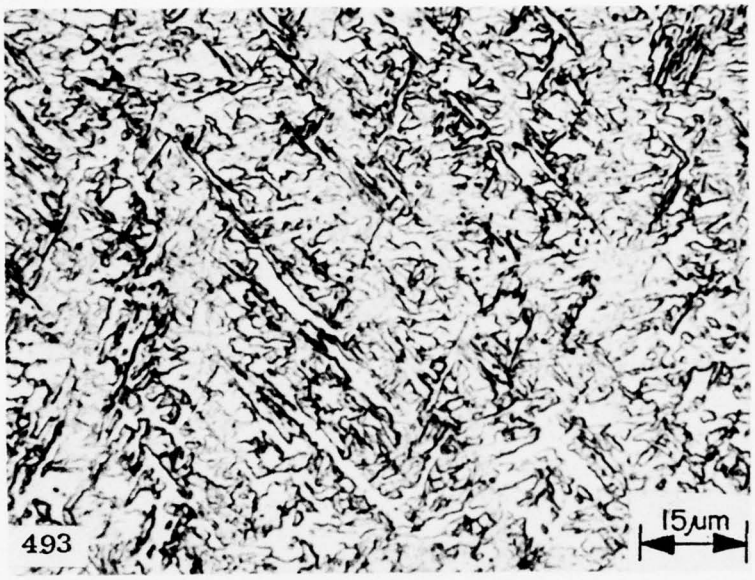

Fig. 7 — Acicular ferrite and martensite in weld metal of 6.35-mm-thick HY-130 SMA weldment. Hardness 38.0 Rc. Etched in 1% nital.

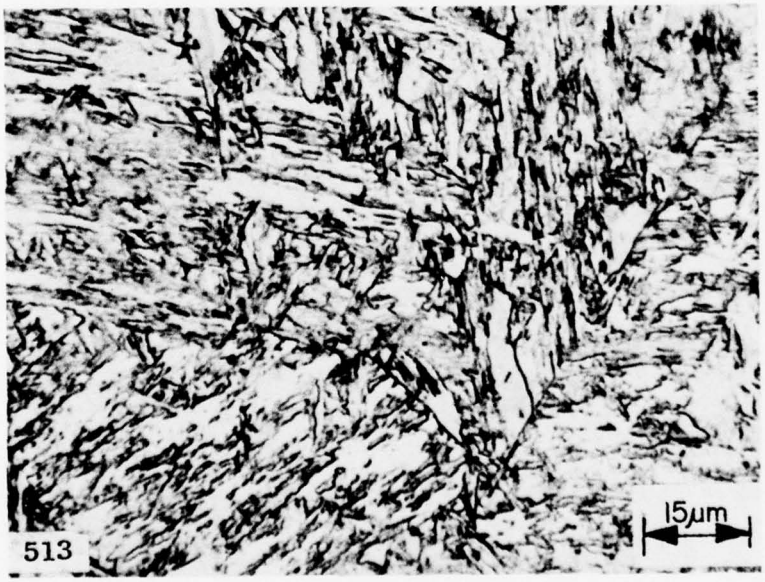

Fig. 8 — Acicular ferrite, martensite, and bainite in weld metal of 6.35-mm-thick GMA weldment. Hardness 37.5 Rc. Etched in 1% nital.

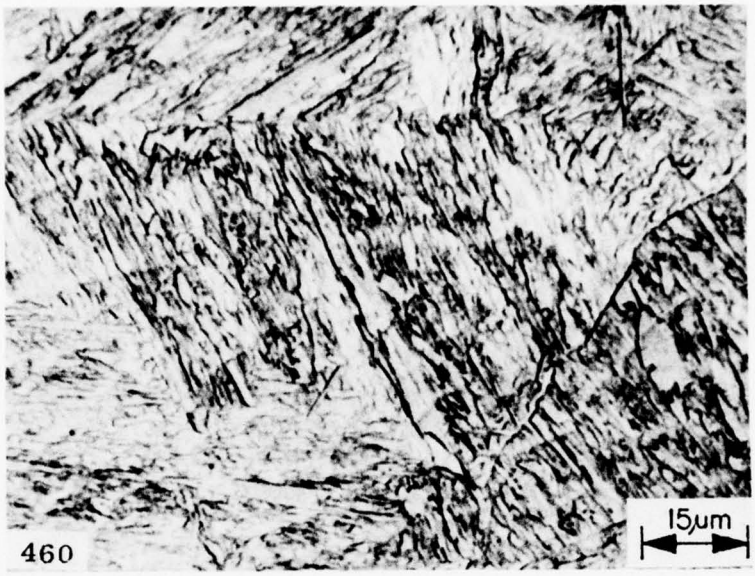

Fig. 9 — Martensite and some bainite in weld metal of 6.35 mm thick EB weldment. Hardness 43.0 Rc. Etched in 1% nital.

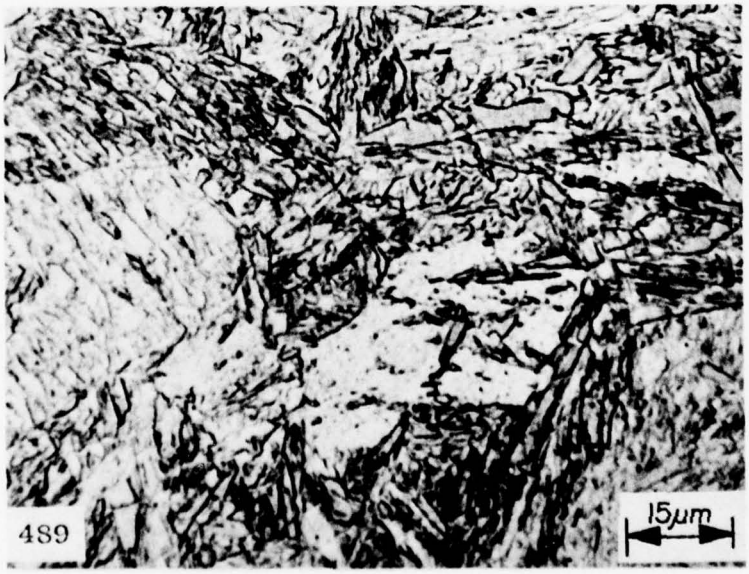

Fig. 10 — Martensite and some bainite in weld metal of 6.35-mm-thick LB weldment. Hardness 42.0 Rc. Etched in 1% nital.

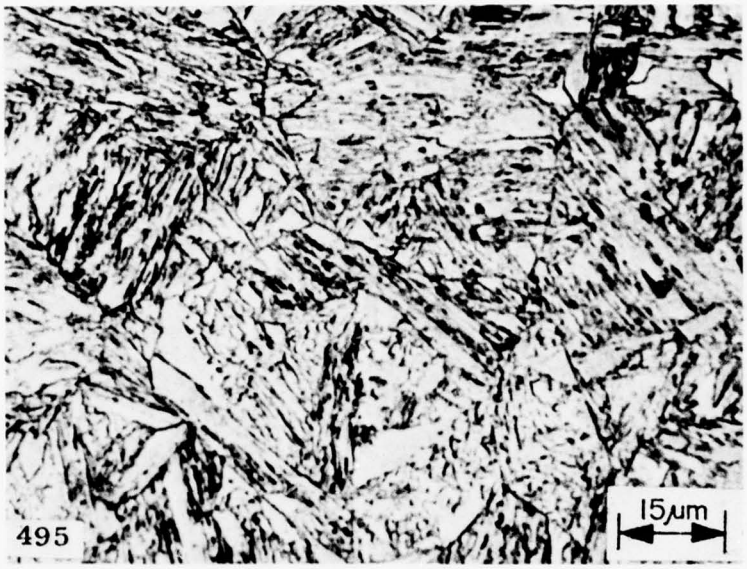

Fig. 11 — Bainite in coarse grain region of HAZ adjacent to fusion boundary in 6.35-mm-thick HY-130 SMA weldment. Hardness 36.5 Rc. Etched in 1% nital.

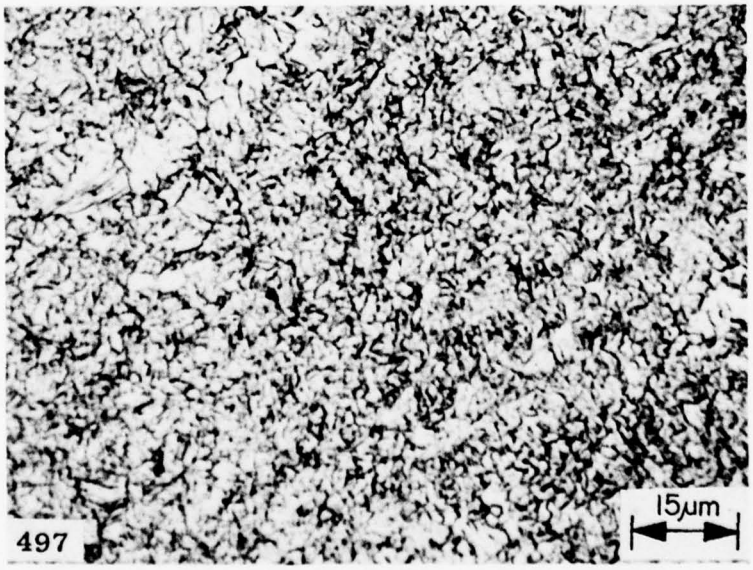

Fig. 12 — Autotempered martensite and some ferrite in fine grain region of HAZ in 6.35-mm-thick HY-130 SMA weldment. Hardness 40.5 Rc. Etched in 1% nital.

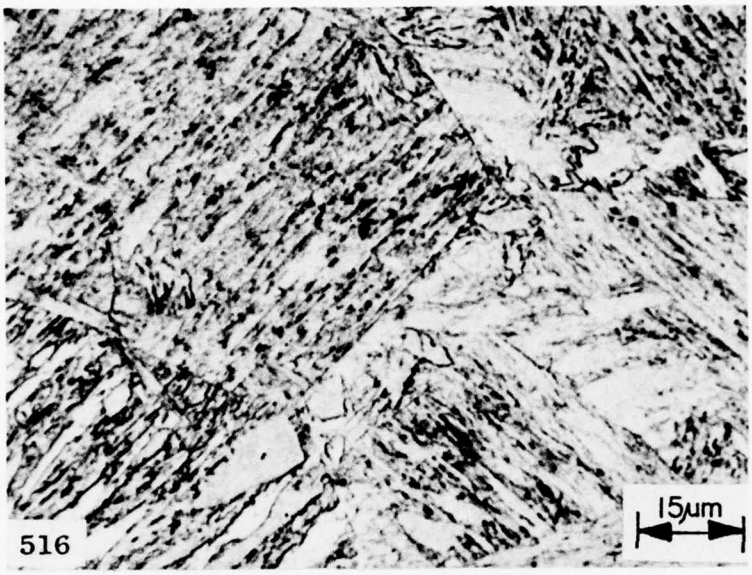

Fig. 13 — Bainite and some acicular ferrite in coarse grain region of HAZ adjacent to fusion boundary in 6.35-mm-thick HY-130 GMA weldment. Hardness 37.5 Rc. Etched in 1% nital.

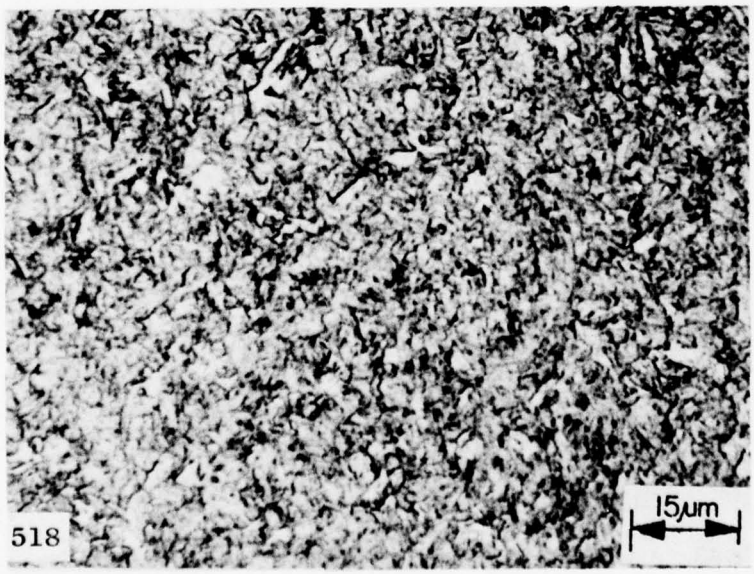

Fig. 14 — Autotempered martensite and some ferrite in fine grain region of HAZ in 6.35-mm-thick HY-130 GMA weldment. Hardness 43.5 Rc. Etched in 1% nital.

Fig. 15 — Martensite and some bainite in medium grain region of HAZ adjacent to fusion boundary in 6.35-mm-thick HY-130 EB weldment. Hardness 40.5 Rc. Etched in 1% nital.

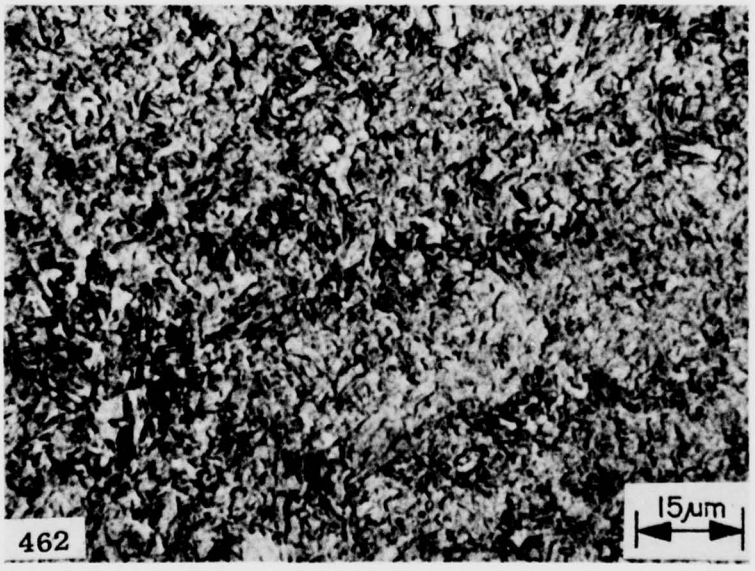

Fig. 16 — Martensite and some ferrite in fine grain region of HAZ in 6.35-mm-thick HY-130 EB weldment. Hardness 45.5 Rc. Etched in 1% nital.

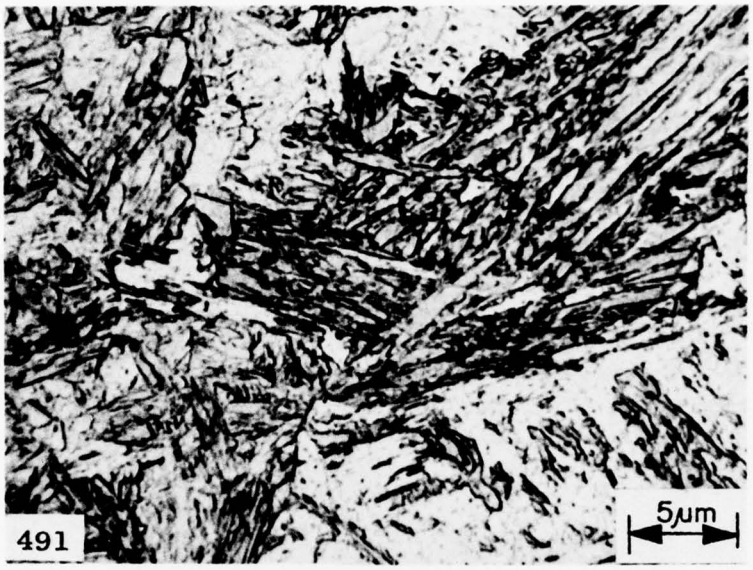

Fig. 17 — Martensite and some bainite in medium grain region of HAZ adjacent to fusion boundary in 6.35-mm-thick HY-130 LB weldment. Hardness 40.5 Rc. *Etched in* 1% nital.

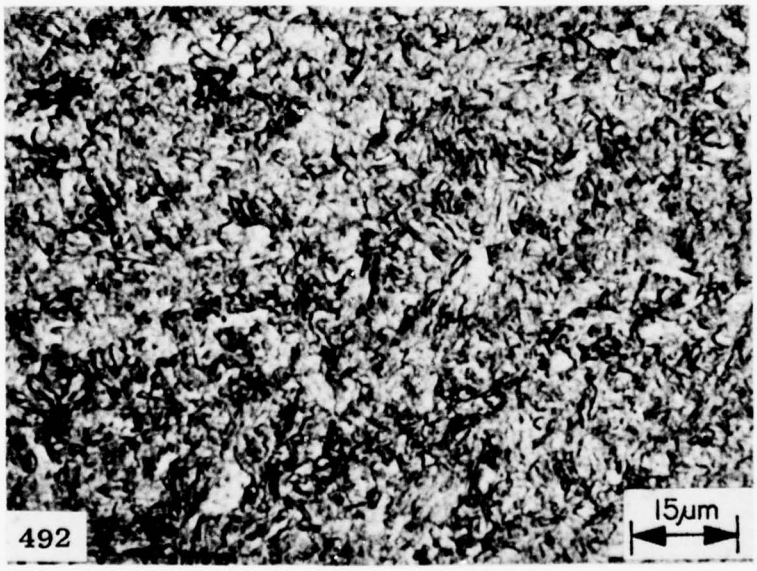

Fig. 18 — Martensite and some ferrite in fine grain region of HAZ in 6.35-mm-thick HY-130 LB weldment. Hardness 44.0 Rc. Etched in 1% nital.

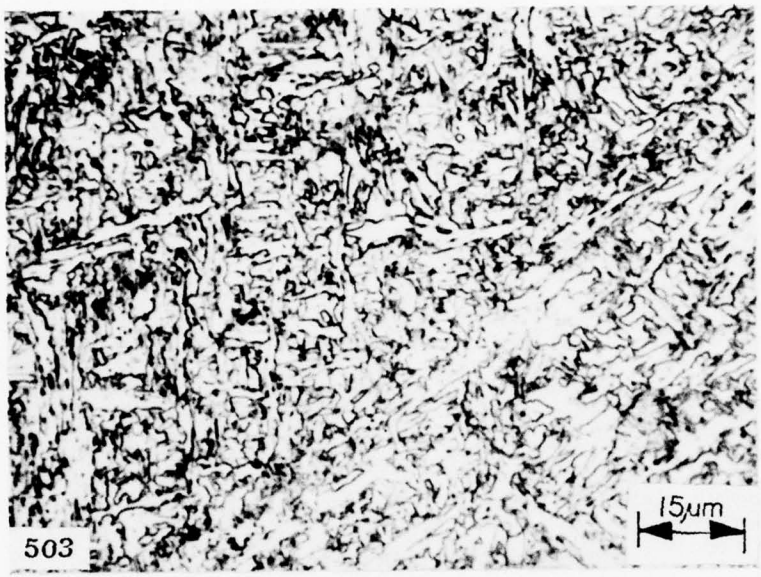

Fig. 19 — Acicular ferrite in weld metal of 12.7-mm-thick HY-130 SMA weldment. Hardness 26.0 Rc. Etched in 1% nital.

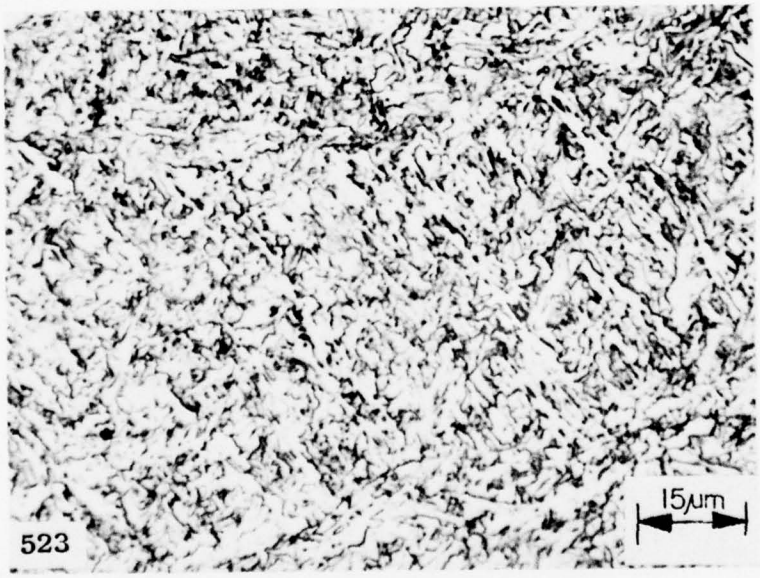

Fig. 20 — Acicular ferrite in weld metal of 12.7-mm-thick HY-130 GMA weldment. Hardness 33.0 Rc. Etched in 1% nital.

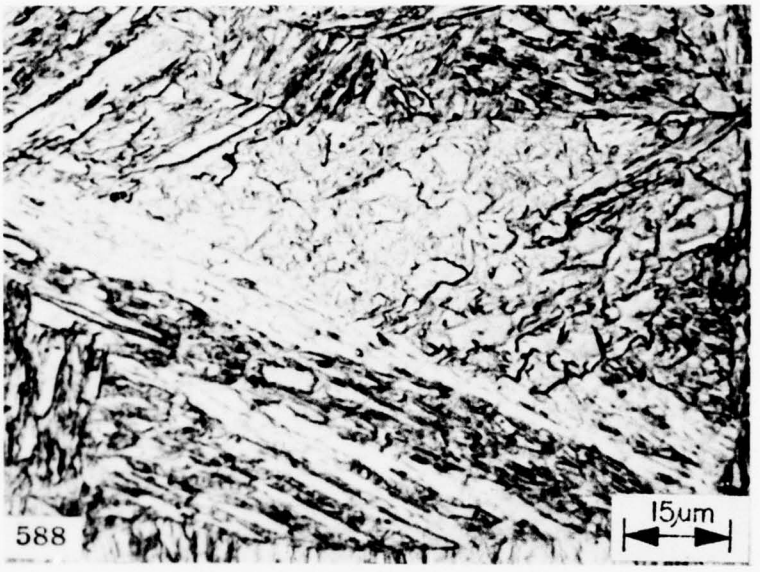

Fig. 21 — Martensite and bainite in weld metal of 12.7-mm-thick HY-130 *EB weldment*. Hardness 37.5 Rc. Etched in 1% nital.

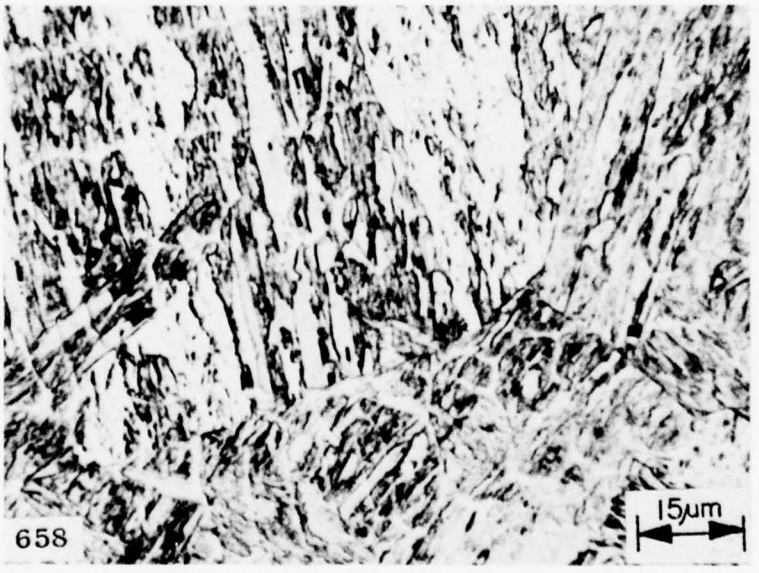

Fig. 22 — Martensite and bainite in weld metal of 12.7-mm-thick HY-130 LB weldment. Hardness 38.5 Rc. Etched in 1% nital.

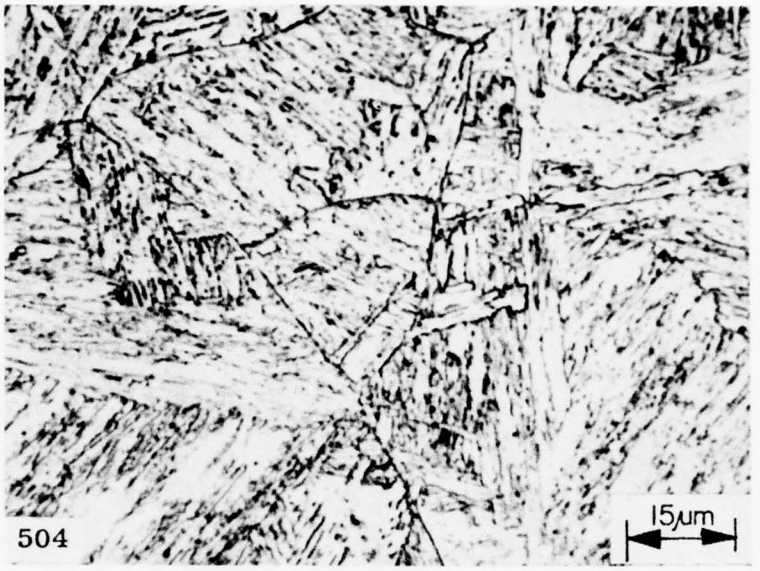

Fig. 23 — Bainite in coarse grain region of HAZ adjacent to fusion boundary in 12.7-mm-thick HY-130 SMA weldment. Hardness 31.0 Rc. Etched in 1% nital.

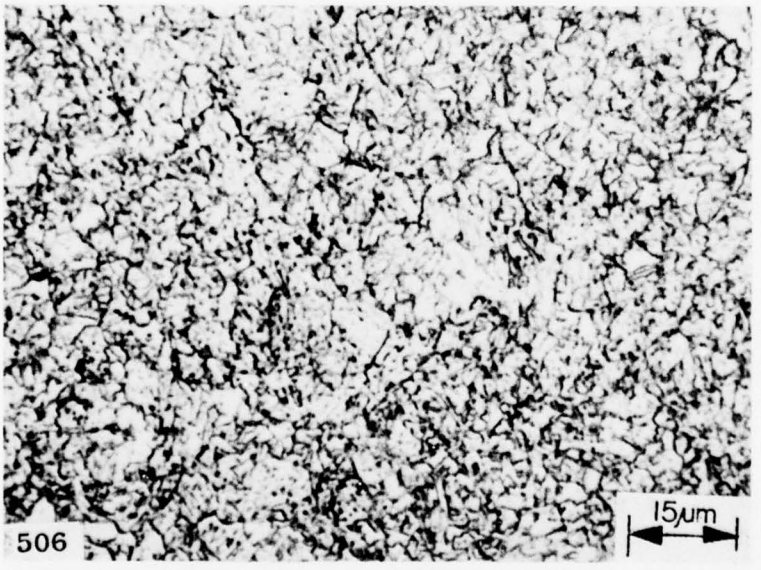

Fig. 24 — Autotempered martensite and ferrite in fine grain region of HAZ in 12.7-mm-thick HY-130 SMA weldment. Hardness 35.0 Rc. Etched in 1% nital.

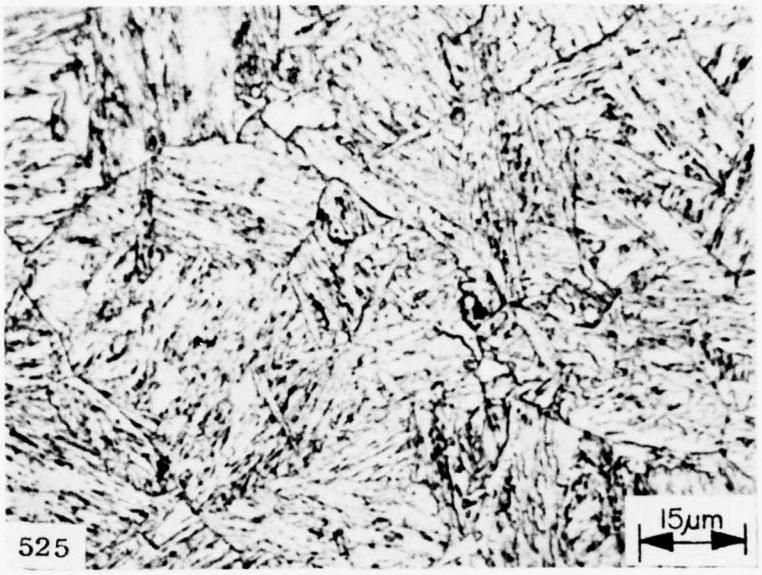

Fig. 25 — Bainite in coarse grain region of HAZ adjacent to fusion boundary in 12.7-mm-thick HY-130 GMA weldment. Hardness 33.0 Rc. Etched in 1% nital.

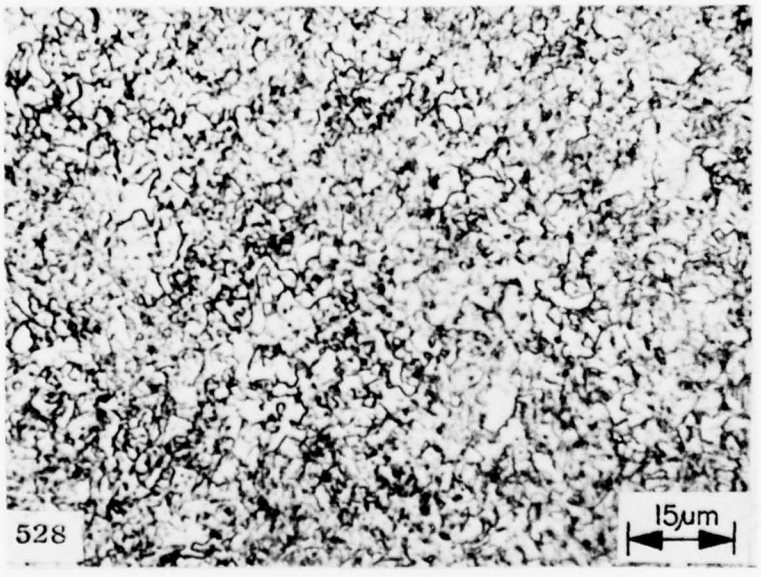

Fig. 26 — Autotemperted martensite and ferrite in fine grain region of HAZ in 12.7-mm-thick HY-130 GMA weldment. Hardness 34.0 Rc. Etched in 1% nital.

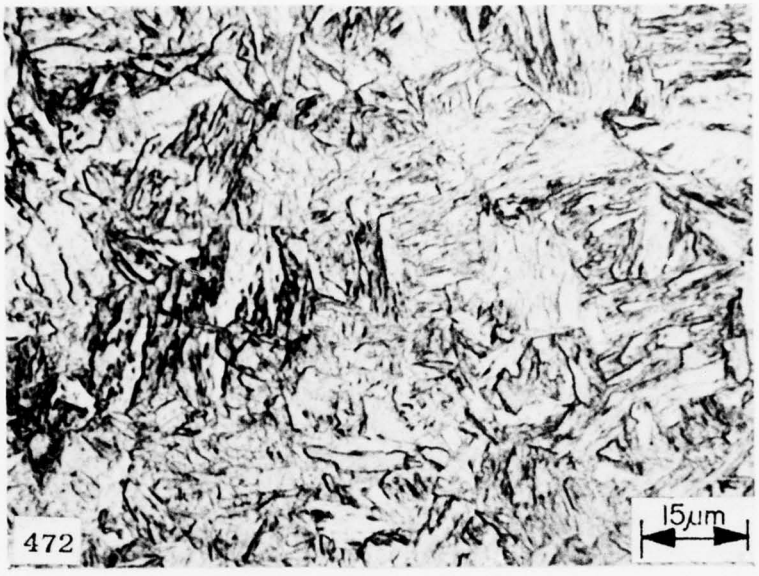

Fig. 27 — Martensite and some bainite in medium grain region of HAZ adjacent to fusion boundary in 12.7-mm-thick HY-130 EB weldment. Hardness 38.0 Rc. Etched in 1% nital.

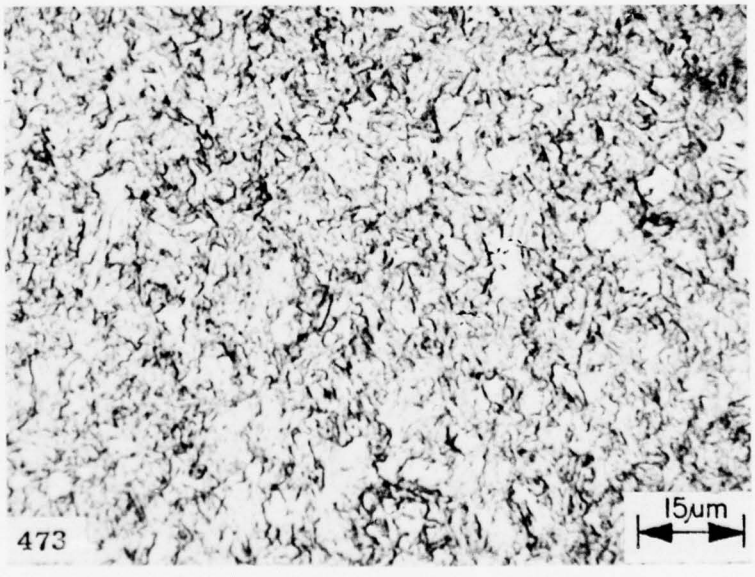

Fig. 28 — Martensite and some ferrite in fine grain region of HAZ in 12.7-mm-thick HY-130 EB weldment. Hardness 41.0 Rc. Etched in 1% nital.

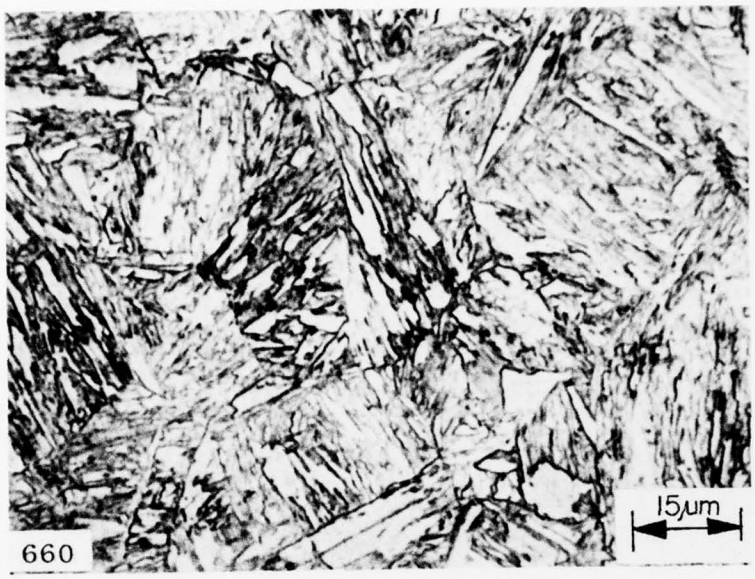

Fig. 29 — Martensite and some bainite in medium grain region of HAZ adjacent to fusion boundary in 12.7-mm-thick HY-130 LB weldment. Hardness 41.0 Rc. Etched in 1% nital.

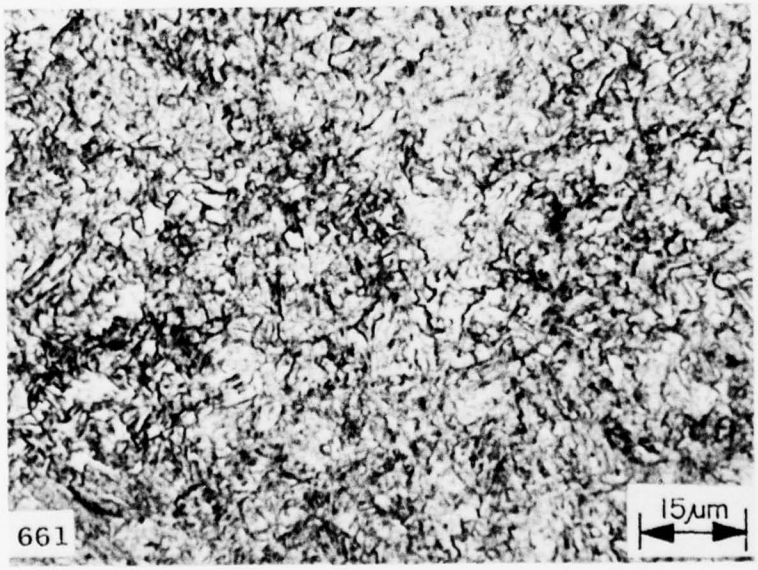

Fig. 30 — Martensite and some ferrite in fine grain region of HAZ in 12.7-mm-thick HY-130 LB weldment. Hardness 43.5 Rc. Etched in 1% nital

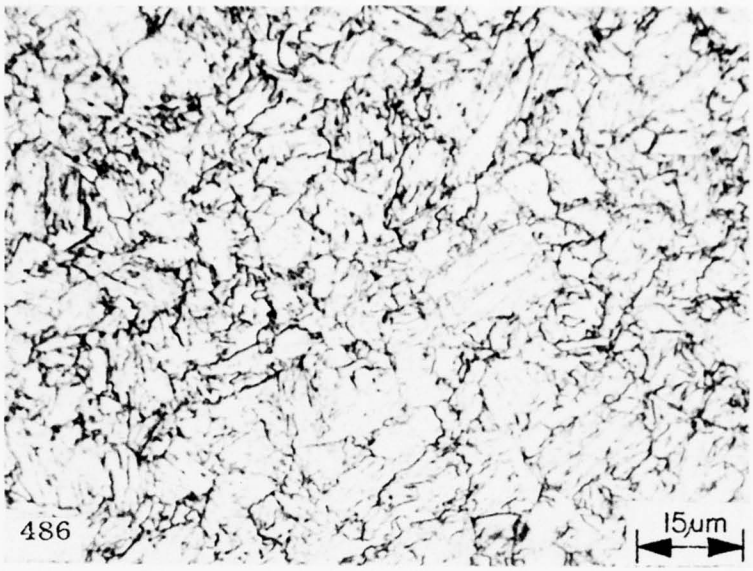

Fig. 31 — Tempered martensite in unaffected base metal of 6.35-mm-thick HY-130 weldment. Hardness 34.0 Rc. Etched in 1% nital.

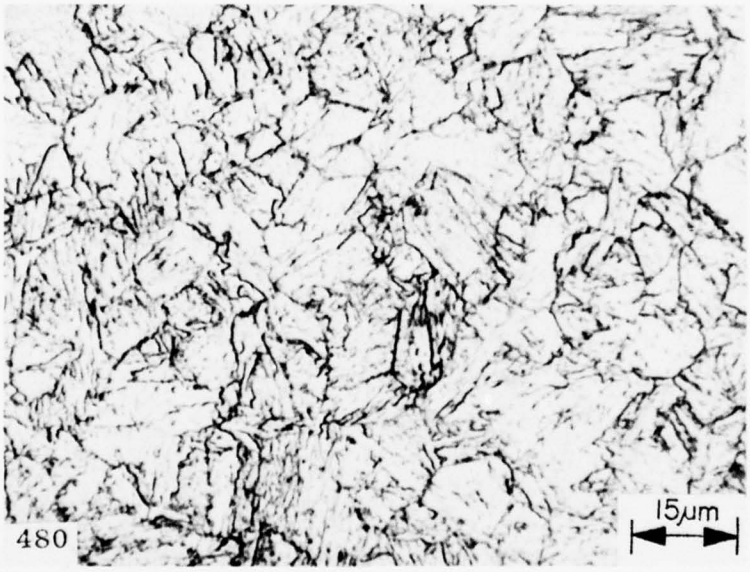

Fig. 32 — Tempered martensite in unaffected base metal of 12.7-mm-thick HY-130 weldment. Hardness 32.0 Rc. Etched in 1% nital.

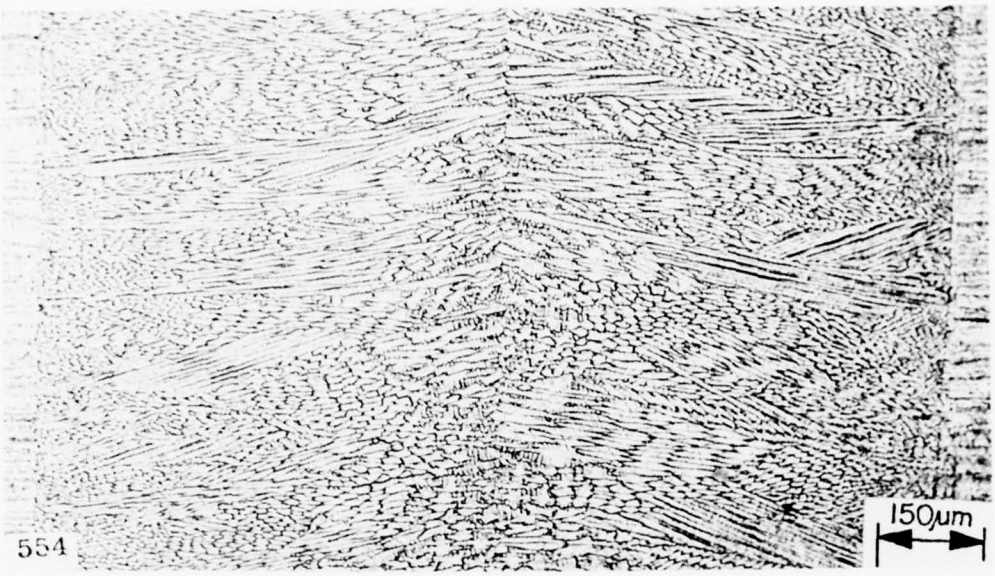

Fig. 33 — Solidification structure of weld metal at midthickness of 6.35-mm-thick HY-130 EB weldment preheated ~ 120°C. Etched in 0.5% ammonium persulphate.

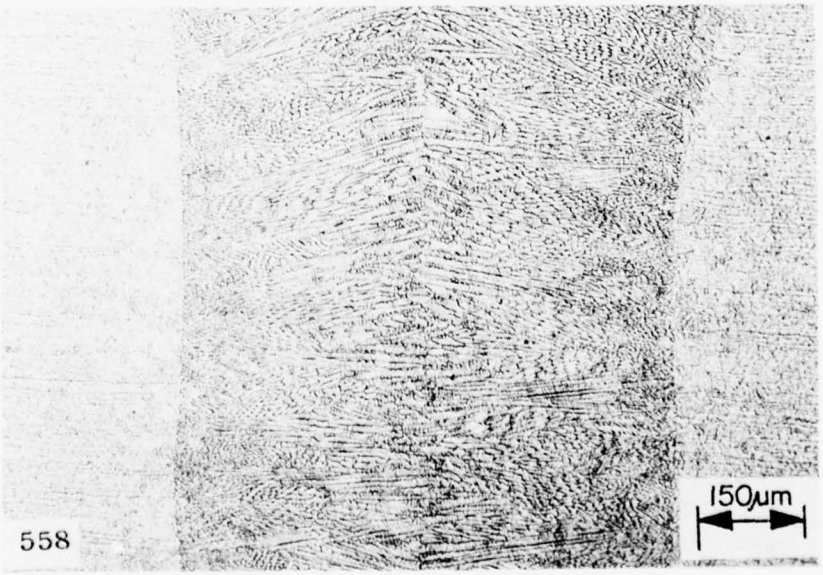

Fig. 34 — Solidification structure of weld metal at midthickness of 6.35-mm-thick LB weldment. Etched in 0.5% ammonium persulphate.

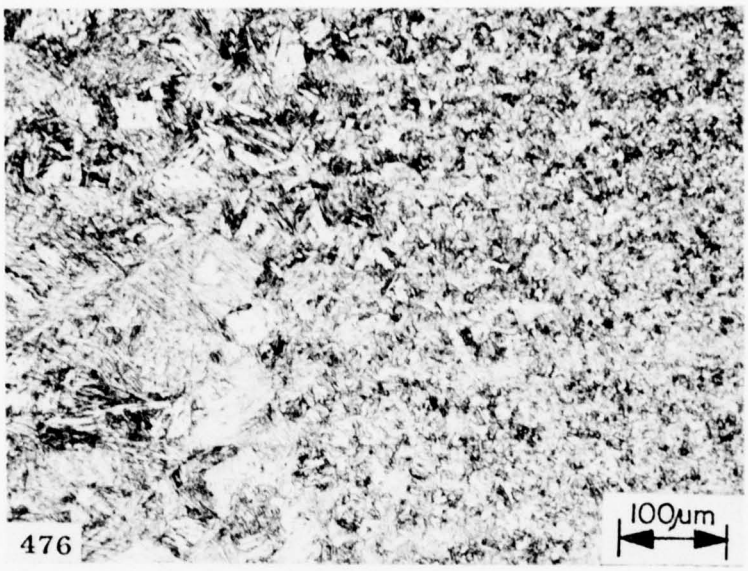

Fig. 35 — Weld metal-HAZ interface of 12.7-mm-thick HY-130 EB weldment preheated ~ 120°C. Etched in 1% nital.

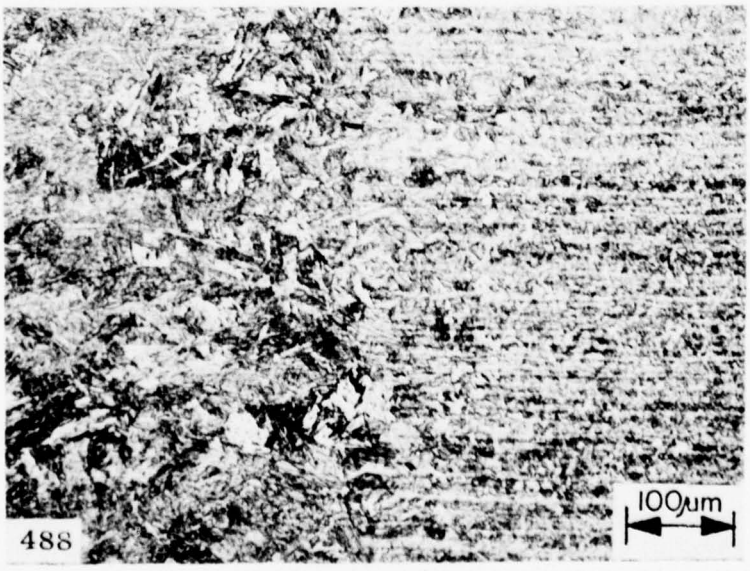

Fig. 36 — Weld metal-HAZ interface of 6.35-mm-thick HY-130 LB weldment. Heat input 0.47 kJ/mm. Etched in 1% nital.

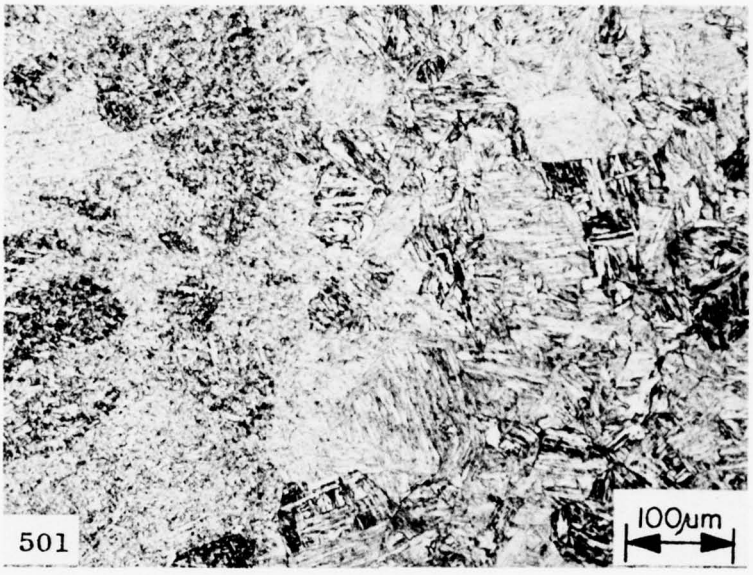

Fig. 37 — Weld metal-HAZ interface of 12.7-mm-thick HY-130 SMA weldment. Etched in 1% nital.

the stress-strain curves beyond 0.2% yield was attained for the weld metal of these joints. Because of the relatively short extension of these curves beyond 0.2% yield, the strain hardening exponent values obtained from the stress-strain data, in some instances, may not be relevant.

Fracture Resistance Properties

Fracture energy data for the 6.35- and 12.7-mm thick DT specimens are compiled in Tables 8 and 9. Presented in the tables are DT energy, R_p, and average hardness values for the base metal and weld joint specimens. The R_p parameter provides an intrinsic and qualitative measure of the fracture toughness of the materials. The parameter was obtained from the empirical equation $E = R_p (\Delta a)^2 B^{1/2}$, where E is the fracture energy, Δa the fracture length, and B the thickness of the specimen [1]. The R_p values in Tables 8 and 9, therefore, reveal in terms of a common denominator the variations in fracture resistance not only between the weld joint and base metal fracture of each thickness but also the markedly wide variations in fracture resistance between the 6.35- and 12.7-mm thicknesses.

Examination of the fractures of the DT specimens (including the base metal specimens) revealed a large measure of plane stress (slant) fracture with flat fracture in the pop-in region and the area near the terminus of the fracture. In many cases small amounts of flat fracture were found to occur in the region midway between the pop-in and the fracture terminus. GMA and LB weld joint fractures of 6.35-mm thickness are shown in Fig. 38, whereas base metal, GMA weld joint, and LB weld joint fractures of 12.7-mm thickness are demonstrated in Fig. 39. Fracture modes, in all instances, including fractures in the flat pop-in region of

Table 6 — Average Tensile Properties of 6.35-mm-Thick Weldments

Specimens	Fracture Location	0.2% YS*		UTS		% Elonga-tion	% Reduc-tion of Area	Strain Hard Exponent*	Mod. of Elasticity*		Hard-ness* (Rc)
		(MPa)	(ksi)	(MPa)	(ksi)				(GPa)	(10^6 psi)	
Base metal	—	971.5	140.9	1014.3	147.1	13.3	63.3	0.025	197.9	28.7	34.0
SMA weld joint	Weld metal	799.1	115.9	997.0*	144.6*	7.2*	42.8*	0.084	201.3	29.2	33.5
GMA weld joint	Base metal	1017.0	147.5†	1019.8	147.9	10.3	58.9	—	208.2	30.2	37.5
EB weld joint	Base metal	994.3	144.2	1019.0	147.8	13.0	60.2	0.027	193.0	28.0	39.0
LB weld joint‡	Base metal	962.0	139.5	1022.1	148.2	12.6	62.0	0.066	190.5	27.6	40.0

*Weld metal values
†Single value
‡Not preheated. Other weldments preheated ~ 120° C.

Table 7 — Average Tensile Properties of 12.7-mm-Thick HY-130 Weldments

Specimens	Fracture Location	0.2% YS*		UTS		% Elonga-tion	% Reduc-tion of Area	Strain Hard Exponent*	Mod. of Elasticity*		Hard-ness* (Rc)
		(MPa)	(ksi)	(MPa)	(ksi)				(GPa)	(10^6 psi)	
Base metal	—	919.8	133.4	959.1	139.1	20.5	72.7	0.026	195.1	28.3	32.0
SMA weld joint	Weld metal	811.5	117.7	943.9*	136.9*	13.1*	52.6*	0.060	197.9	28.7	29.0
GMA weld joint	Base metal	916.3	132.9	955.6	138.6	17.0	73.1	0.048	193.7	28.1	34.0
EB weld joint	Base metal	907.4	131.6	941.2	136.5	18.5	73.7	0.031	197.9	28.7	37.5
EB weld joint†	Base metal	909.5	131.9	946.0	137.2	18.5	74.2	0.027	203.4	29.5	38.0
LB weld joint†	Base metal	846.5	122.8	960.3	139.3	18.9	74.3	0.077	190.5	27.6	40.0

*Weld metal values
†Not preheated. Other weldments preheated ~ 120° C.

Table 8 — Fracture Resistance Data of 6.35-mm-Thick HY-130 Weldments*

Specimens	DT Energy Range		Av DT Energy		R_p		Av Hardness (Rc)	
	(ft-lb)	(N·m)	(ft-lb)	(N·m)	$\frac{\text{ft lb}}{\text{in. 5/2}}$	$\frac{\text{MN·m}}{\text{m 5/2}}$	Weld Metal	HAZ
Base metal	342.0-415.0	464.0-563.0	391.0	530.0	437.1	5.8	34	
SMA weld joint	293.0-358.0	397.0-485.0	334.0	453.0	373.4	4.9	33.5	37.5
GMA weld joint	264.0-305.0	358.0-414.0	285.0	386.0	319.0	4.2	37.5	40.5
EB weld joint	273.0-307.0	370.0-416.0	287.0	389.0	321.0	4.2	39.0	42.5
EB weld joint**	267.0-348.0	362.0-472.0	308.0	418.0	344.3	4.5	39.5	43.0
LB weld joint**	351.0-447.0	476.0-606.0	382.0	518.0	427.1	5.6	40.0	41.5

*Specimens were tested in a two-ply configuration of 6.35-mm-thick laminates.
**Not preheated. Other weldments preheated ~ 120°C.

Table 9 — Fracture Resistance Data of 12.7-mm-Thick HY-130 Weldments

Specimens	DT Energy Range		Av DT Energy		R_p		Av Hardness (Rc)	
	(ft-lb)	(N·m)	(ft-lb)	(N·m)	$\frac{\text{ft lb}}{\text{in. 5/2}}$	$\frac{\text{MN·m}}{\text{m 5/2}}$	Weld Metal	HAZ
Base metal	759.0-881.0	1029.0-1194.5	804.0	1090.0	899.0	11.9	32	
SMA weld joint	475.0-560.0	644.0- 759.0	524.0	710.5	586.0	7.7	29.0	33.0
GMA weld joint	420.0-663.0	569.5- 899.0	515.0	698.0	576.0	7.6	34.0	33.0
EB weld joint	536.0-739.0	727.0-1002.0	662.0	897.5	740.0	9.8	37.5	38.0
EB weld joint*	585.0-634.0	793.0- 859.5	610.0	827.0	682.0	9.0	38.0	39.5
LB weld joint*	567.0-948.0	769.0-1285.0	760.0	1030.0	850.0	11.2	40.0	41.0

*Not preheated. Other weldments preheated ~ 120°C.

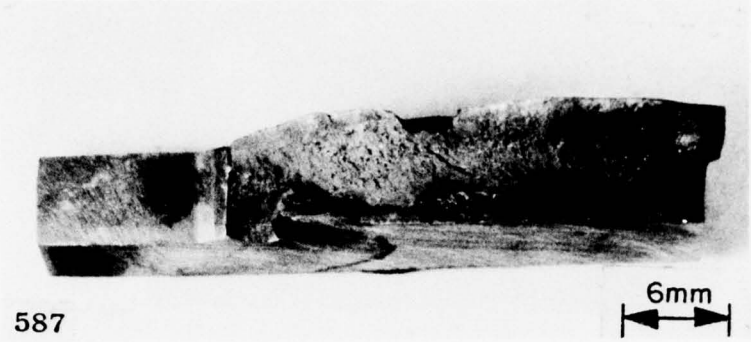

(a) GMA weld joint

(b) LB weld joint

Fig. 38 — Single laminates of DT fractures of 6.35-mm-thick HY-130 weld joint specimens.

the weld metal, were identified as those of microvoid coalescence. Microvoid coalescence among the different weld joints generally showed variations in dimple size as indicated below:

- SMA and GMA weld joint fractures (both thicknesses)
  - Medium to fine dimples in pop-in region (Figs. 40 and 41)
  - Medium to coarse dimples in weld metal at midthickness (Fig. 42)
  - Medium to fine dimples in weld metal near surface (Fig. 43)

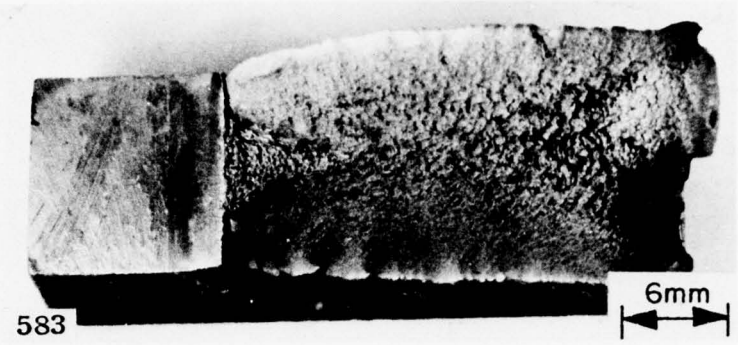

(a) Base metal

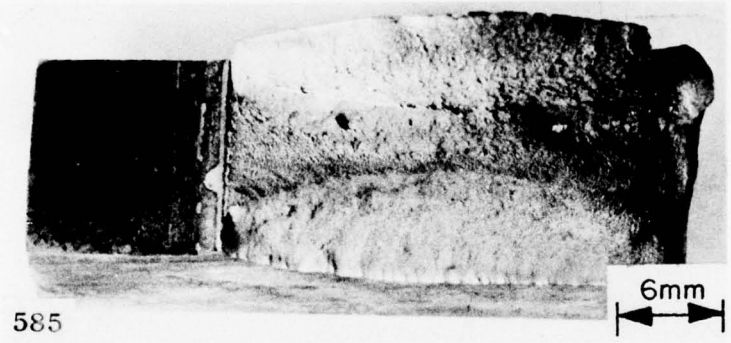

(b) GMA weld joint

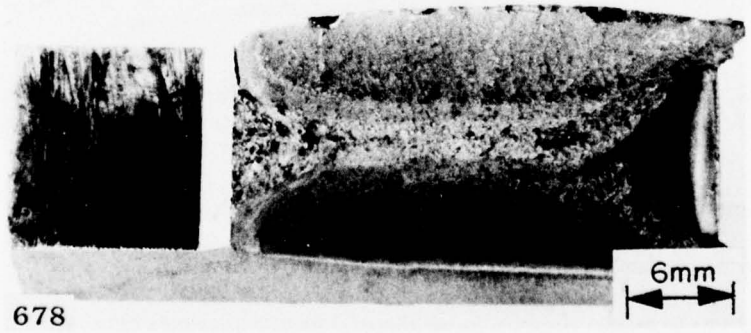

(c) LB weld joint.

Fig. 39 — DT fractures of 12.7-mm-thick HY-130 base metal and weld joint specimens.

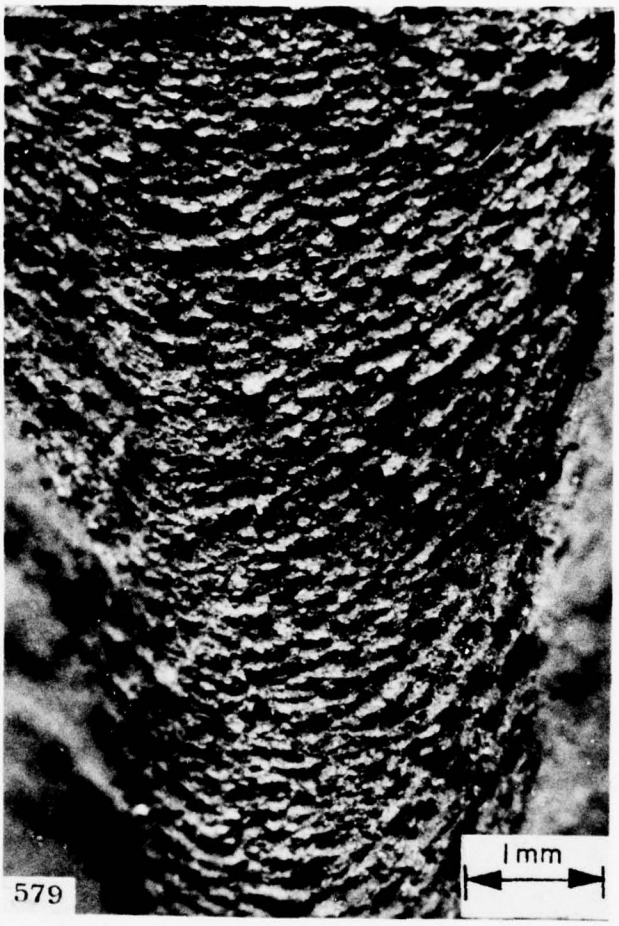

Fig. 40 — Pop-in region in weld metal of GMA weld joint fracture of 12.7-mm-thick HY-130 DT specimen.

- EB and LB weld joint fractures (both thicknesses)
  - — Medium to coarse dimples in pop-in region (Figs. 44 and 45)
  - — Medium to fine dimples in weld metal at midthickness (Fig. 46)
  - — Mostly fine dimples in unaffected base metal (Fig. 47)

Light fractographs revealed that the pop-in regions of the EB and LB weld joint fractures were similar in appearance to the pop-in regions of the base metal specimens; Fig. 44 shows this for the weld joints, and Fig. 48 illustrates it for the base metal specimens. Note evidence of gas pockets in the pop-in region of the EB weld (Fig. 44). This type of porosity also was evident in the LB welds but to a more limited degree.

Fig. 41 — Microvoid coalescence in pop-in region in weld metal of GMA weld joint fracture of 12.7-mm-thick HY-130 DT specimen.

Fig. 42 — Microvoid coalescence in weld metal in midthickness region of GMA weld joint fracture of 12.7-mm-thick HY-130 DT specimen.

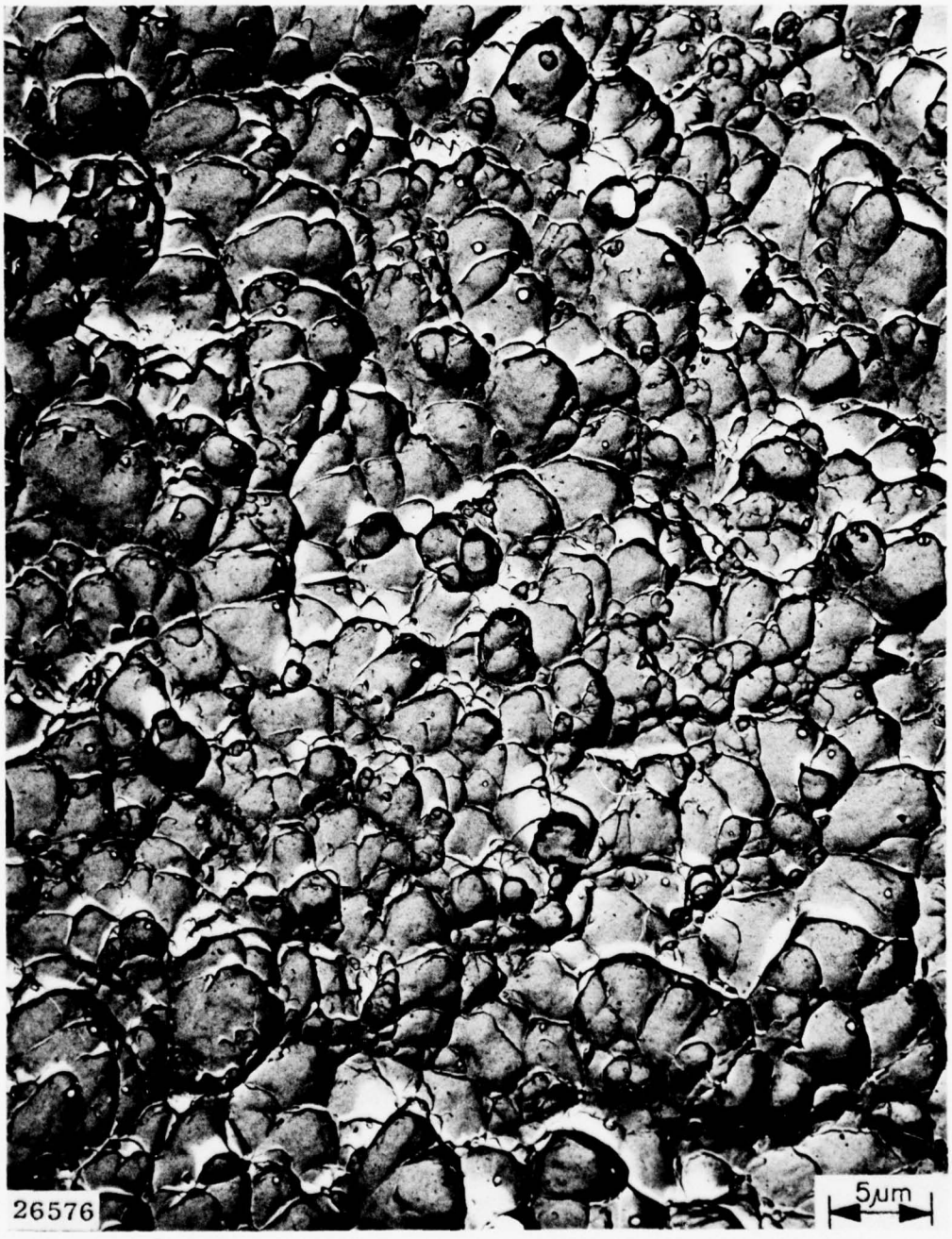

Fig. 43 — Microvoid coalescence in weld metal near surface of GMA weld joint fracture of 12.7-mm-thick HY-130 DT specimen.

Fig. 44 — Pop-in region in weld metal of EB weld joint fracture of 12.7-mm-thick HY-130 DT specimen. Preheated ~ 120°C. Note gas pockets in fracture.

The weld joint fractures may be termed "composite fractures" because of the inclusion, generally, of the following components: (a) weld metal and HAZ in the SMA and GMA weld joints; and (b) weld metal, HAZ, and unaffected base metal in the EB and LB weld joints. The extent to which the composite fractures are made up of these components may best be discovered by examining the fracture profiles of the weld joint specimens as depicted in Fig. 49 for the 12.7-mm thick SMA and LB weld joints. The fracture profile covers the lateral span of the fracture and is revealed in a transverse cross section cut preferably from the midpoint region of the fracture (between the base of the notch and the terminus of the fracture). The length of weld metal, HAZ, or unaffected base metal in the fracture profile divided by the overall span of the profile indicates the proportion of these components in the composite fracture. The percentages of these metals in the composite fractures of the different weld joints are given in Table 10.

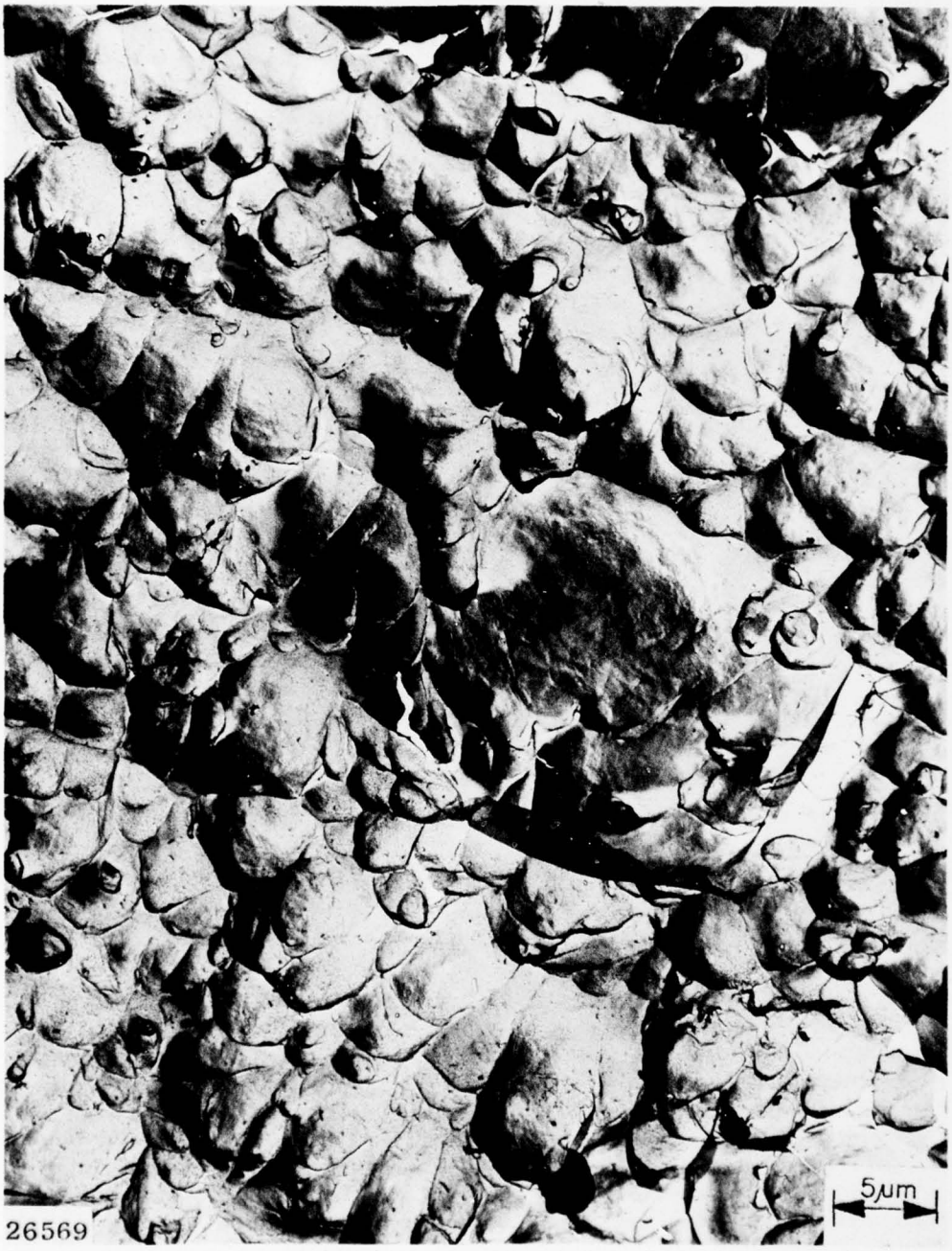

Fig. 45 — Microvoid coalescence in pop-in region in weld metal of EB weld joint fracture of 12.7-mm-thick HY-130 DT specimen. Not preheated.

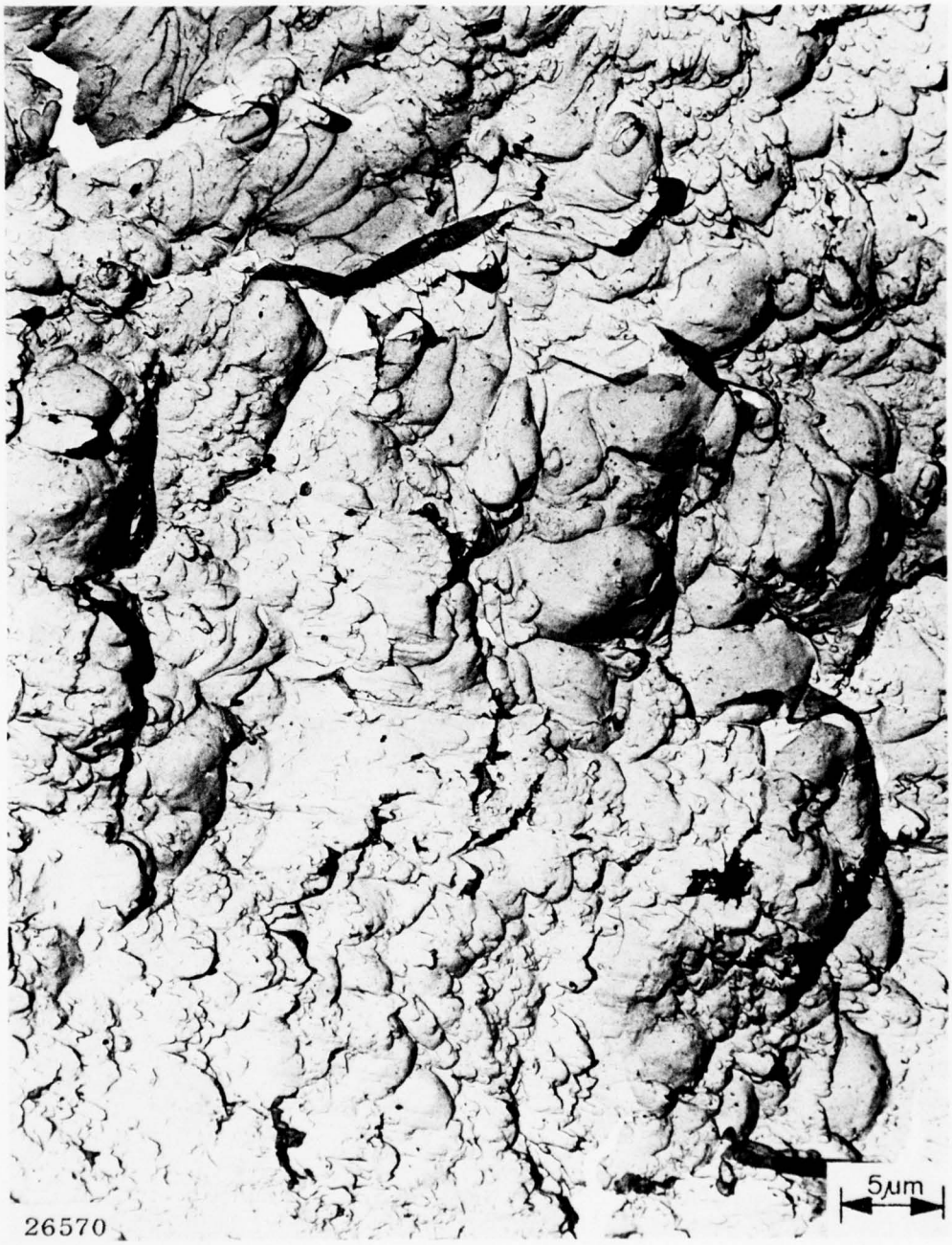

Fig. 46 — Microvoid coalescence in weld metal in midthickness region of EB weld joint fracture of 12.7-mm-thick HY-130 DT specimen. Not preheated.

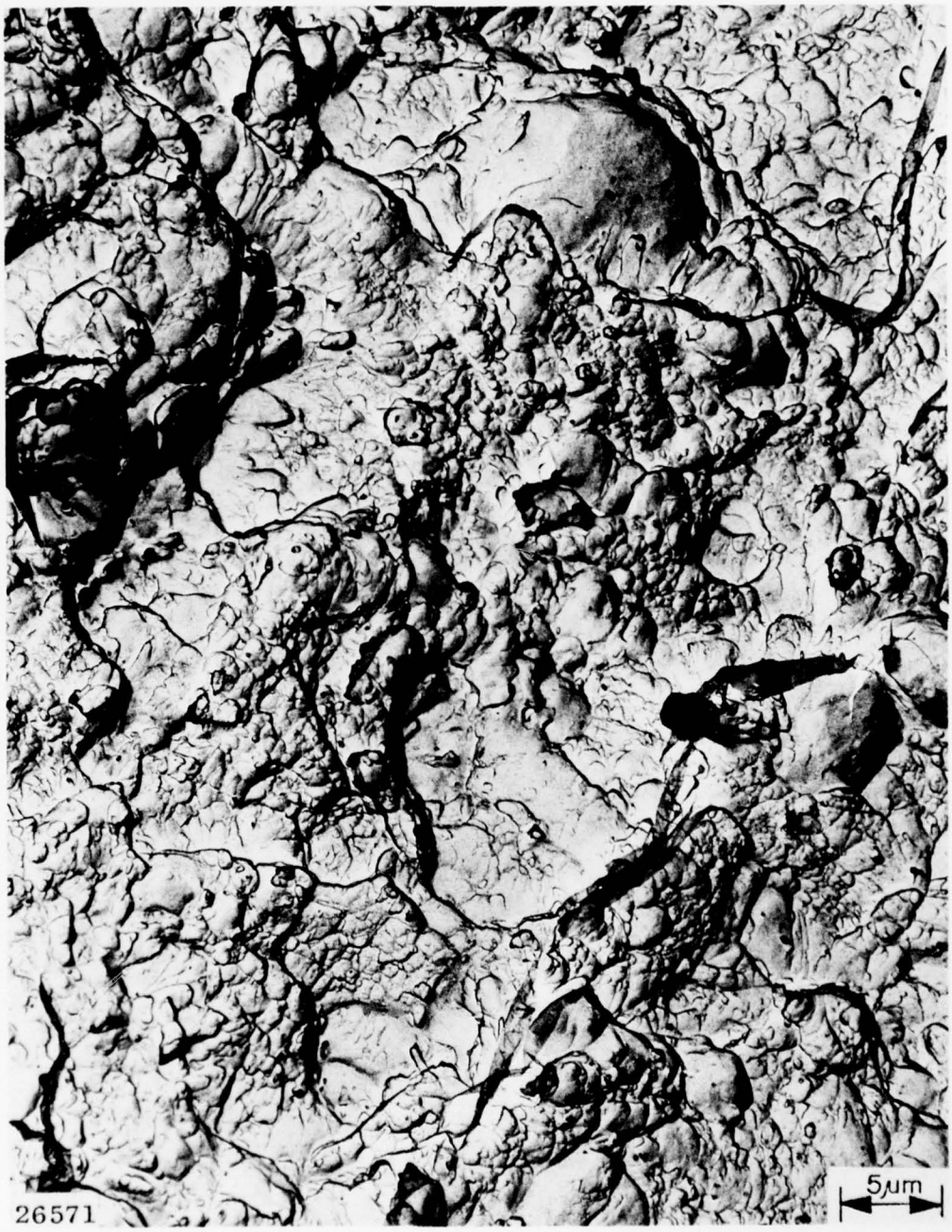

Fig. 47 — Microvoid coalescence in unaffected base metal in EB weld joint fracture of 12.7-mm-thick HY-130 DT specimen. Not preheated.

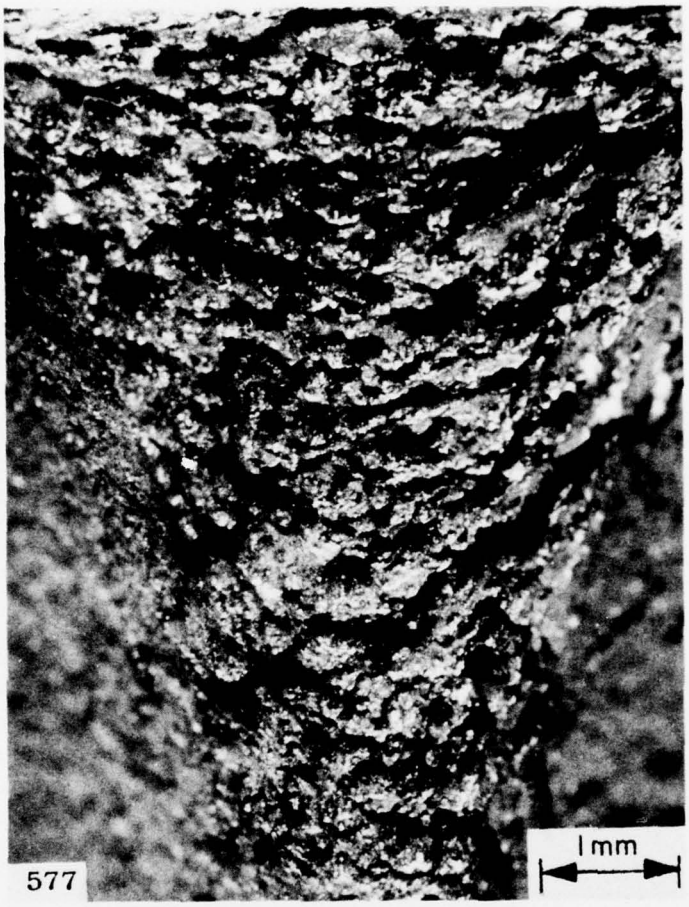

Fig. 48 — Pop-in region of fracture in 12.7-mm-thick base metal DT specimen.

Of the 6.35-mm thick weld joints tested, the GMA and EB (preheated) specimens showed the lowest values of fracture resistance, as indicated in Table 8. The 6.35-mm-thick SMA and GMA weld joints disclosed fractures of moderate porosity. The fractures had a somewhat sharp and irregular appearance, which is illustrated by the GMA fracture in Fig. 38. The low fracture resistance of the 6.35-mm-thick GMA weld joints was believed attributable to porosity and the presence of a relatively high percentage of HAZ in the fracture (see Table 10). The unusually low fracture toughness found in the 6.35-mm-thick EB specimens was due largely to the formation of cold shuts (incomplete fusion), as shown in Fig. 50. These specimens, however, showed less evidence of porosity than the EB specimens of 12.7-mm thickness. The 6.35-mm-thick LB weld joints revealed little porosity. Some evidence of incomplete fusion, however, was detected in one LB weld joint specimen.

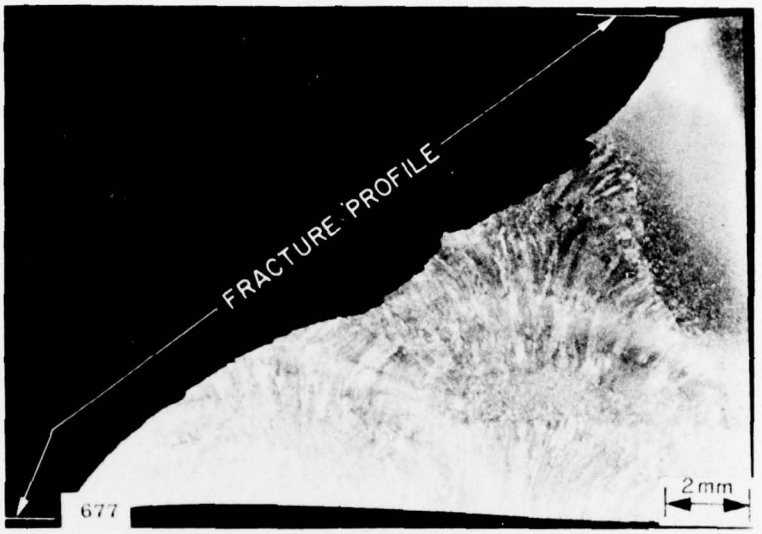

(a) SMA weld joint

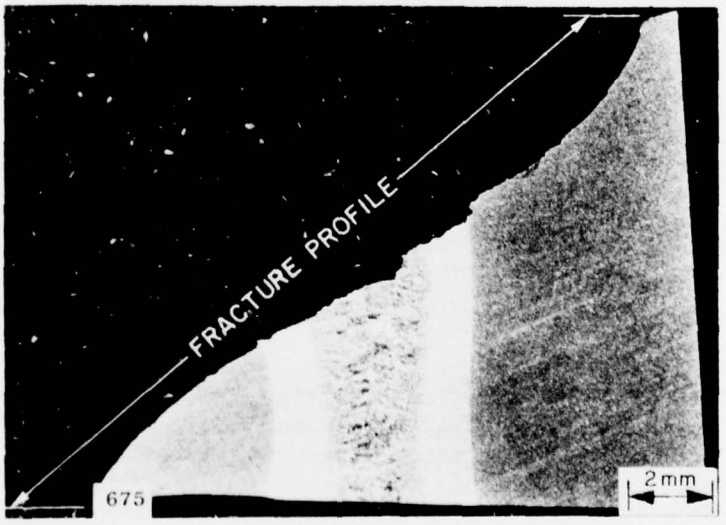

(b) LB weld joint.

Fig. 49 — Fracture profiles of 12.7-mm-thick HY-130 weld joint fractures.

Table 10 — Average Percentages of Components in Composite Fractures of 6.35- and 12.7-mm-Thick Weldments

Weld Joints	% Weld Metal		% HAZ		% Unaffected Base Metal	
	6.35 mm	12.7 mm	6.35 mm	12.7 mm	6.35 mm	12.7 mm
SMA	98.1	77.9	1.9	22.1	0	0
GMA	46.0	84.4	54.0	15.6	0	0
EB	20.5	9.0	19.0	10.4	60.5	80.6
LB*	17.6	17.1	23.5	15.7	58.9	67.1

*Not preheated. Other weldments preheated ~ 120°C.

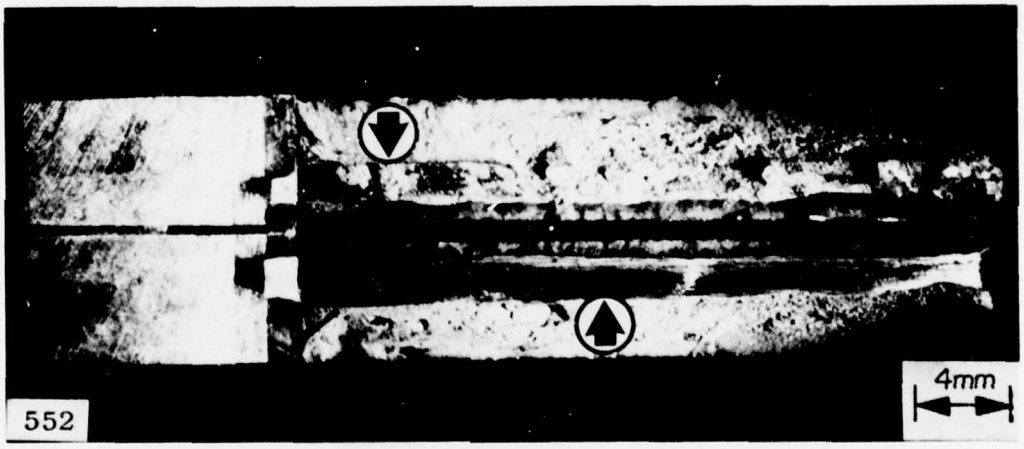

Fig. 50 — Arrows show cold shuts (incomplete fusion) in fracture of two-ply HY-130 EB weld joint DT specimen. Each ply is 6.35 mm thick. Not preheated.

Among the 12.7-mm thicknesses tested, the lowest values of fracture resistance were disclosed for the SMA and GMA weld joints (see Table 9). Porosity (light to moderate) and a perceptible amount of flat fracture in the weld metal contributed in some measure to the low fracture toughness of these weld joints. The 12.7-mm-thick EB weld joints showed evidence of more porosity and a greater degree of flat fracture than the corresponding LB weld joint specimens. Incomplete fusion also was found in the 12.7-mm-thick EB weld joint specimens but to a more limited extent than in the EB specimens of 6.35-mm thickness (see Fig. 51).

The LB weld joints showed the highest average fracture resistance of the different weld joint specimens tested in both thicknesses. As shown in Tables 8 and 9, the fracture energies of the LB weld joints include values both higher and lower than average base metal

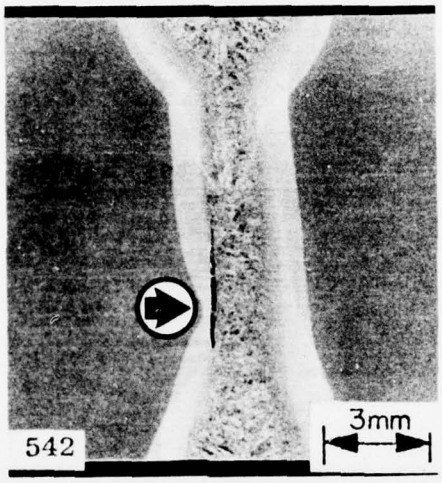

Fig. 51 — Cold shut (incomplete fusion) shown on transverse cross section of 12.7-mm-thick HY-130 EB weld joint. Preheated ~ 120°C.

values. In a comparable study, Breinan and Banas [2] found the fracture resistance of 6.40-mm thick HY-130 LB welds to be equivalent to or better than that of the base metal. They linked the high fracture toughness of the LB welds to a reduction of the inclusion content at the fusion zone. In Table 11, the 6.35- and 12.7-mm-thick LB weld joints show 97.7 and 94.5 percent equivalences to the base metal fractures. The GMA weld joints revealed the lowest equivalences of 72.9 and 64.0 percent, respectively. Intrinsically, as revealed by the R_p parameters, the fracture resistances of the 12.7-mm thicknesses are about twice those of the 6.35-mm thicknesses.

A hydrogen flake was detected on the fracture surface of a dynamic-tear, 12-7-mm-thick, LB weld joint specimen. The flake, shown in Figs. 52 and 53, was located in the weld metal between the pop-in region above it and a highly ruptured (porous) region below it. Transmission electron microscope (TEM) and scanning electron microscope (SEM) fractographs of the flake reveal evidence of intergranular fracture (Figs. 54 and 55). As shown in Fig. 56, the fracture mode of the ruptured area below the flake is microvoid coalescence. The DT value (788 N·m) of the specimen was substantially below the average DT value (1030 N·m) for the 12.7-mm-thick LB weld joint specimens.

Table 11 — Fracture Resistance Assessment of 6.35- and 12.7-mm-Thick HY-130 Weldments

Weld Joints	Percent Equivalence to Base Metal	
	6.35 mm	12.7 mm
SMA	85.4	65.2
GMA	72.9	64.0
EB	73.4	82.3
EB*	78.8	75.9
LB*	97.7	94.5

*Not preheated. Other weldments preheated ~ 120°C.

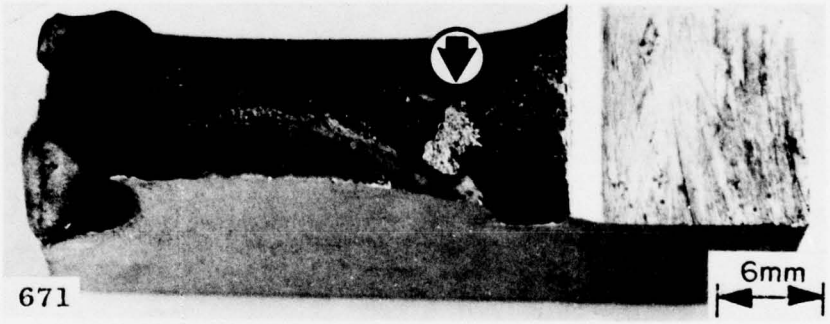

Fig. 52 — Hydrogen flake on fracture surface of LB weld in 12.7-mm-thick HY-130 DT specimen

ANALYSIS OF RESULTS

The 6.35- and 12.7-mm base metal thicknesses revealed high yield strength-ultimate tensile strength (YS-UTS) ratios of 95.7 and 95.9, respectively, which were reflected by low strain hardening exponent values of 0.025 and 0.026. In contrast, the SMA welds of 6.35- and 12.7-mm thicknesses showed YS-UTS ratios of 80.1 and 85.9 with correspondingly high strain hardening values of 0.084 and 0.060. However, since fracture took place in the base metal, no ultimate tensile strengths were obtained for the GMA, EB, and LB welds from the tests of the weld joint specimens. The comparatively high strain hardening values (0.048 to 0.077) obtained for the GMA and LB welds are believed to indicate correctly, on the basis of direct relationship of hardness to tensile strength, that the potential ultimate tensile strengths of these welds are substantially higher than their actual yield strengths. On the other hand, although the low strain hardening values (0.027 and 0.031) for the 12.7-mm-thick EB welds suggest an ultimate tensile strength not appreciably higher than their yield strength of ~ 909 MPa (132 ksi), it is evident from their relatively high hardness of ~ 38 Rc that a substantially higher nominal ultimate tensile strength is called for. These probable discrepancies in strain hardening values for the 12.7-mm-thick EB welds are believed

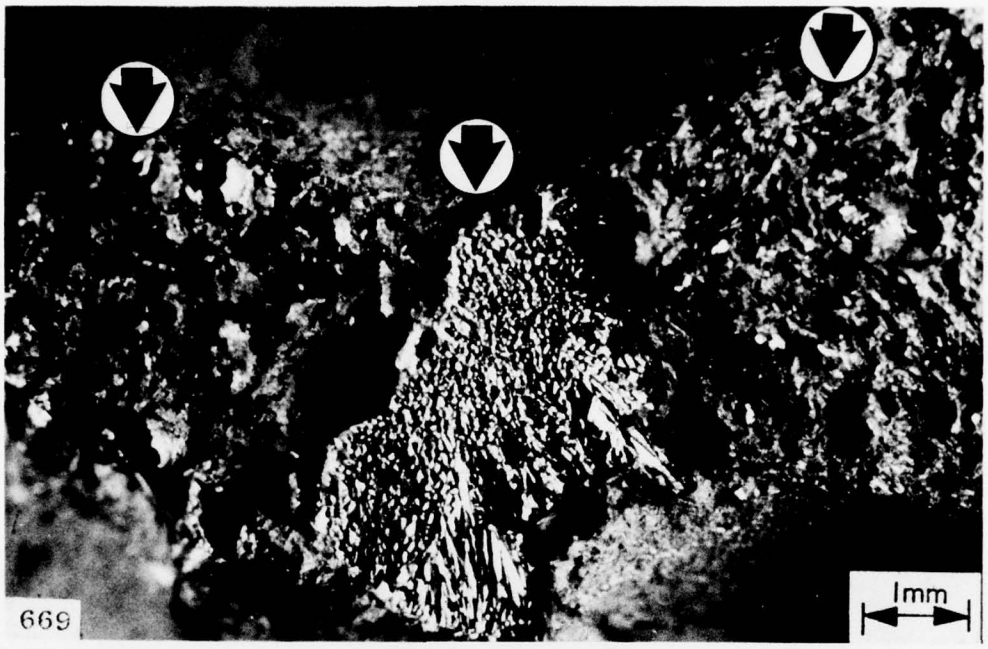

Fig. 53 — Enlarged view of Fig. 52 showing: (left) highly fissured region below flake (center) and (right) pop-in region above flake

attributable to the limited extension of the stress-strain curves of these welds beyond 0.2% yield. The attainment of greater extension of these curves before the onset of fracture might have made it feasible to construct a more accurate slope for measuring the strain hardening parameters.

It is not unusual to find marked variations in fracture resistance among different heats of wrought steel of the same chemical specifications. These variations can occur even though the materials are heat treated in the same way and notched similarly in regard to rolling direction [3]. A wide divergence in fracture toughness is revealed between the 6.35- and 12.7-mm-thick plates, as shown in Tables 8 and 9. The R_p parameter forthe 12.7-mm-thick base metal discloses an intrinsic fracture toughness one order of magnitude greater than that of the 6.35-mm thickness. An interesting aspect of this disclosure is that the fracture toughnesses of the 12.7-mm-thick weld joints differ from those of 6.35-mm thickness also by approximately one order of magnitude. These variations are disclosed by the R_p ratios presented in Table 12. It may be inferred from these R_p ratios that the quality of the weld joint from the standpoint of fracture resistance can be no better than that of the unaffected base metal. In most instances, the weld joint would not be expected to exceed the base metal in fracture resistance regardless of how low the fracture resistance of the plate might be.

Fig. 54 — TEM fractograph showing intergranular fracture in hydrogen flake detected in LB weld of 12.7-mm-thick HY-130 DT specimen

Fig. 55 — SEM fractograph showing intergranular fracture in hydrogen flake detected in LB weld of 12.7-mm-thick HY-130 DT specimen

As shown in Table 10, the presence of high percentages of unaffected base metal in the fracture of the LB weld joints reasonably indicates that the greater share of the high fracture toughness of these weld joints was contributed by the unaffected base metal. This same trend in high fracture toughness should be manifested for the EB weld joints since these weldments also show fractures with high percentages of unaffected base metal. However, lower fracture toughnesses were obtained for the EB weld joints, particularly those of 6.35-mm thickness, due in large measure to the formation of cold shuts at the weld-HAZ interface, as illustrated in Fig. 51. Such defects are difficult to detect by radiographic inspection [4]. The cold shuts represent, essentially, intrinsic cracks in the weld joints. With imposition of internal and external stresses, these cracks could very well propagate along the weld-HAZ interface. The cold shuts could also be sources of stress corrosion [5].

Because of the small percentage of weld metal in the LB weld joint fractures, it is difficult to make a definite assessment of the fracture toughness of the weld metal per se, but one can observe that the weld metal is at least comparable to the base metal in fracture toughness. This would be strongly indicated by the high percentile values of the LB weld joints (see Table 11). Fractures of the LB weld joints correspond to upper shelf values on curves showing fracture energy and fracture mode transition temperatures. These upper

Fig. 56 — Microvoid coalescence in highly fissured region below hydrogen flake in LB weld of 12.7-mm-thick HY-130 DT specimen

Table 12 — R_p Ratios of Weld Joints

Weld Joint	$\frac{R_p \text{ of 12.7-mm}}{R_p \text{ of 6.35-mm}}$
Base Metal	2.0
SMA	1.6
GMA	1.8
EB	2.3
EB*	2.0
LB*	2.0

*Not preheated. Other weldments preheated ~ 120°C.

shelf fractures portray the characteristic plane stress (slant fracture) configuration of ductile materials. If the LB weld metal does have greater fracture resistance than the base metal, it may be more effectively revealed by testing base metal and weld joint specimens over a range of temperatures (subzero to ambient temperatures). The fracture transition characteristics of the weld and base metals would be more selectively identified by such testing, especially at those temperatures where the metals are more conducive to plane strain (flat) fracture.

Potential sources of hydrogen that caused the flake found in the LB weld metal of the 12.7-mm-thick dynamic tear specimen (Figs. 52 and 53) might be moisture adsorbed on the surface of the plates that were welded or possibly moisture contamination from the shielding gases. Hydrogen is believed to have been produced either by the dissociation of water vapor or more likely by the surface reaction of water vapor and metal ($H_2O + Fe \rightleftharpoons FeO + 2H$). In this process liberated hydrogen was dissolved in the molten metal to form the flake which represents an area of high hydrogen concentration. The fissured region adjacent to the flake might be due to passage of water vapor, methane, or hydrogen sulphide through the melt. The gases could have been formed by reaction of excess hydrogen with oxygen, carbon, or sulphur in the metal [6]. Because of their insolubility in the melt, these gases could very likely have caused a severe bubbling or boiling action in the metal. That the fracture mode (Fig. 56) of this region was microvoid coalescence might indicate that there was little or no lattice absorption of hydrogen in the ruptured metal.

The metallurgical conditions and variables that promote susceptibility to cold cracking in the fabrication of HY-130 weldments are more prevalent in the multipass SMA and GMA weldments than in the single-pass EB and LB weldments. The SMA and GMA weldments are more likely to be subjected to a high degree of shrinkage, distortion, grain coarsening, and thermal cycling effects, which may create a wide coverage of residual stresses and sometimes high stress concentrations. When metal of limited ductility can no longer accommodate these stresses, the susceptibility to cold cracking may be very high. The EB and LB weldments will generally incur a minimum amount of distortion and shrinkage. The narrow weld and heat-affected zones of these weldments are of relatively high hardness and have grains that are medium to fine. Only a limited area for build-up of residual stresses is

provided. Potential hydrogen absorptions may occur in all weldments and, with special empahsis on SMA weldments, can give rise to embrittlement and development of microcracks in weld metal and HAZ.

The hardness traverses for the SMA and GMA weld joints in Figs. 5 and 6 reveal no wide variations in hardness or steep hardness gradients. In contrast, the EB and LB weld joints demonstrate high hardnesses and steep hardness gradients, which may indicate the presence of sizable stress concentrations. However, along with the high hardnesses in the latter weld joints, there is also present a relatively fine grain size. The combination of high hardness and fine grain size constitutes what may be termed a beneficial synergistic effect, which imparts strength and toughness to the weld joints sufficient to withstand the build-up of high stresses. On the contrary, when high hardness is combined with a coarse grain size, then high stress concentrations can impose deleterious effects. Bernstein and Thompson [7] have shown that in low alloy steels resistance to hydrogen cracking is improved by (a) a refined grain size and/or (b) a tempered martensite structure. Tempered bainite was revealed to be more susceptible to fracture than tempered martensite. Although tempering is not indicated in Tables 4 and 5, martensitic structures of the EB and LB weld joints were subjected to some degree of tempering at relatively low temperatures. This tempering action was due to heat developed in the welding operation.

In all weldment fabrications, regardless of the process used, susceptibility to cold cracking can be decreased substantially if the necessary precautions are taken in regard to the following items: (a) cleanliness as related to grinding dust, flux entrapment, scale, oil, and grease; (b) maintenance of proper preheating and interpass temperatures; (c) effective moisture elimination from plates, covered electrodes, filler rod, and shielding gases; and (d) appropriate upkeep and utilization of welding equipment.

SUMMARY OF RESULTS

1. Weldments of 6.35-mm thickness were found to have somewhat higher hardness than weldments of 12.7-mm thickness because of the greater hardenability of the thinner plates. The EB and LB welds were perceptibly harder than the SMA and GMA welds. Average weld metal hardnesses of the SMA and GMA welds ranged from 29.0 to 37.5 Rc, and those of the EB and LB welds from 37.5 to 40.0 Rc. Hardness traverses across the heat-affected zones revealed noticeably steeper hardness gradients in the EB and LB weldments than in the SMA and GMA weldments.

2. The EB and LB welds showed relatively finer grain structures in the weld and HAZ than the SMA and GMA welds.

3. The microstructures of the SMA weldments were found to be similar to those of the GMA weldments. The EB and LB weldments were also similar in microstructure. The former microstructures consisted of a large percentage of acicular ferrite with somewhat smaller percentages of bainite and martensite, whereas the latter microstructures were composed mostly of martensite with smaller amounts of bainite.

4. Fracture of the SMA transverse weld tension specimens took place in the weld metal; the GMA, EB, and LB specimens fractured in the base metal. In both the 6.35- and 12.7-mm thicknesses, the SMA welds showed the lowest yield strength values of 799.1 and

811.5 MPa (115.9 and 117.7 ksi). The GMA welds exhibited the highest yield strength values of 1017.0 and 916.3 MPa (147 5 and 132.9 ksi). The EB and LB yield strengths were at intermediate levels.

5. The SMA, GMA, and LB welds revealed substantially higher strain hardening exponents than the base metal. The values ranged from 0.048 to 0.084 for the welds and 0.025 to 0.026 for the base metal. The strain hardening exponents of the EB welds were comparable to those of the base metal.

6. The DT fractures of the different weld joints, on the whole, revealed mostly plane stress (slant) fractures. However, SMA and GMA weld joints of 6.35-mm thickness exhibited to a large degree fracture of somewhat sharp and irregular appearance.

7. The 6.35- and 12.7-mm-thick LB weld joint specimens showed the highest fracture toughness of all the weld joint specimens tested; the fracture energy equivalences to the base metal were 94.5 and 97.7 percent. As disclosed by examination of the fracture profiles of the specimens, the SMA and GMA fractures, in most instances, consisted predominantly of weld metal with a smaller percentage of HAZ. However, in the case of the EB and LB specimens, the fracture comprised largely unaffected base metal with smaller amounts of weld metal and HAZ. The high percentage of unaffected base metal in these fractures was a strong indication that the greater share of the EB and LB fracture toughnesses was attributable to this base metal component.

8. Metallurgical conditions and variables that promote susceptibility to cold cracking may be more prevalent in the SMA and GMA weldments than in the EB and LB weldments. Some variables involved were hardness, stress, grain size, and microstructure. Deleterious effects of high hardness and steep hardness gradients in the EB and LB weldments may be offset by beneficial synergistic effects producing high hardness and a relatively fine grain size.

9. The SMA and GMA weldments showed no outright manifestations of hydrogen embrittlement but did reveal evidence of a relatively small to moderate amount of porosity. The most prominent defects observed in the EB weldments were cold shuts (incomplete fusion), whereas in the LB weldments there was evidence on a minor scale of incomplete fusion and hydrogen embrittlement.

ACKNOWLEDGMENTS

The authors express their appreciation to Mr. D. A. Meyn for his assistance and guidance in strain gage instrumentation, to Dr. J. M. Krafft for his advice on work relating to the strain hardening exponent, and to Mr. E. R. Pierpoint for his fractographic work. We are especially grateful to the United Technologies Research Center for fabrication of the LB weldments.

REFERENCES

1. R. W. Judy, Jr., and C. A. Griffis, "Fracture Extension Resistance of Aluminum Alloys in Thin Sections," NRL Report 7627, Oct. 12, 1973.

2. E. M. Breinan and D. M. Banas, "Fusion Zone Purification During Welding with High Power CO_2 Lasers," United Aircraft Research Laboratories Report R111087-2, Apr. 1975.

3. R. W. Judy, Jr., and R. J. Goode, "Fracture Extension Resistance (R-Curve) Characteristics for Three High-Strength Steels," NRL Report 7361, Dec. 30, 1971, p 5.

4. *Metals Handbook*, 8th ed., vol. 6, 1971, p. 539.

5. *Metals Handbook*, 8th ed., vol. 6, 1971, p. 288.

6. G. E. Linnert, ed., *Welding Metallurgy*, 3rd ed., 1967, vol. 2, p. 206, American Welding Society, New York.

7. I. M. Bernstein and A. W. Thompson, "Effect of Metallurgical Variables on Environmental Fracture of Steels," *International Metals Rev.*, **21**, 278-279 (Dec. 1976).

Appendix A

DETERMINATION OF STRAIN HARDENING EXPONENT

The strain hardening exponent shows the rate of increase of stress with increase in plastic strain from 0.2% yield to maximum load on the stress-strain diagram. This part of the stress-strain curve becomes a straight line in a log-log plot and conforms to the relationship $\sigma = K\epsilon^n$, where n is the strain hardening exponent. To obtain n in a log-log plot, the tensile stress P/A_0 is converted to true stress (σ_T) by the equation

$$\sigma_T = \frac{P}{A_0}(1 + \epsilon_T),$$

where

P = load
A_0 = original area
ϵ_T = total strain
$\epsilon_T = \epsilon_E$ (elastic strain) + ϵ_p (plastic strain).

Then σ_T is plotted against ϵ_p. The slope of the straight line becomes the strain hardening exponent n.